# TCC Training Seminar on
# Primary Modes of Global Climate Variability and Regional Climate

**14 – 18 November 2016**

**Tokyo, Japan**


## Tokyo Climate Center
## Japan Meteorological Agency

# TCC Training Seminar on Primary Modes of Global Climate Variability and Regional Climate

**14 – 18 November 2016**
**Tokyo, Japan**

## Contents


**- Schedule of the Training Seminar** **i**
**- List of Participants** **ii**

**(Item 3)**
**- "Introduction to Climatology"**
**for experts on climate services** **1**

**(Item 5)**
**- Interannual to decadal variability in the tropical oceans** **17**

**(Item 6)**
**- Primary modes of variability in Earth's climate system** **27**

**(Item 7)**
**- Introduction of reanalysis and JRA-55** **39**

**Annex**
**- Introduction and operation of iTacs**

# Schedule

# TCC Training Seminar on

## Primary Modes of Global Climate Variability and Regional Climate

### Tokyo, Japan, 14 -18 November 2016

**Draft Schedule**

| | | |
|---|---|---|
| Day 1 - Monday, 14 November | | |
| 10:00-10:40 | 1. Opening<br>- Welcome Address<br>- Self-introduction by participants<br>- Group photo shooting<br>- Courtesy call on JMA's Director-General | |
| 10:40-11:00 | Coffee Break | |
| 11:00-11:15 | 2. Introduction: Outline and scope of the Training Seminar | |
| 11:15-12:30 | 3. Lecture: “Introduction to Climatology” for experts on climate services | |
| 12:30-14:00 | Lunch | |
| 14:00-15:50 | 3. Lecture: “Introduction to Climatology” for experts on climate services | |
| 15:50-16:10 | 4. Lecture: Tokyo Climate Center Website (TCC website) and its products<br>-For monitoring the world climate and ocean- | |
| 16:10-16:30 | Coffee Break | |
| 16:30-17:20 | 5. Lecture: Interannual to decadal variability in the tropical oceans | |
| 17:20-18:10 | 6. Lecture: Primary modes of variability in Earth's climate system | |
| 18:30-20:00 | Reception | at KKR Hotel Tokyo |
| Day 2 - Tuesday, 15 November | | |
| 09:30-10:15 | 7. Lecture: Introduction of reanalysis and JRA-55 | |
| 10:15-11:15 | 8. Exercise: Introduction and operation of iTacs (Basic) | |
| 11:15-11:35 | Coffee Break | |
| 11:35-12:30 | 8. Exercise: Introduction and operation of iTacs (Basic) | |
| 12:30-14:00 | Lunch | |
| 14:00-15:40 | 8. Exercise: Introduction and operation of iTacs (Advanced) | |
| 15:40-16:00 | Coffee Break | |
| 16:00-17:00 | 8. Exercise: Introduction and operation of iTacs (Advanced) | |
| 17:00-18:00 | 9. Lecture: ENSO, AO, and climate in Japan | |
| Day 3 - Wednesday, 16 November | | |
| 9:30-11:00 | 10. Exercise: Finding climate characteristics associated with primary modes of global climate variability | |
| 11:00-11:20 | Coffee Break | |
| 11:20-12:30 | 11. Exercise: Finding statistical relationship between primary modes of variability and atmospheric circulation | |
| 12:30-14:00 | Lunch | |
| 14:00-16:00 | 11. Exercise: Finding statistical relationship between primary modes of variability and atmospheric circulation | |
| 16:00-16:20 | Coffee Break | |
| 16:20-18:00 | 12. Exercise: Considering mechanisms of the relationship between primary modes of climate variability and atmospheric circulation | |
| Day 4 - Thursday, 17 November | | |
| 9:30-11:00 | 12. Exercise: Considering mechanisms of the relationship between primary modes of climate variability and atmospheric circulation | |
| 11:00-11:20 | Coffee Break | |
| 11:20-12:30 | 13: Exercise: Preparation for presentation | |
| 12:30-14:00 | Lunch | |
| 14:00-16:00 | 13: Exercise: Preparation for presentation | |
| 16:00-16:20 | Coffee Break | |
| 16:20-18:00 | 14. Presentation by participants | Presentation (15 min.)<br>followed by Q&A (5 min.) |
| Day 5 - Friday, 18 November | | |
| 09:30-12:10 | 14. Presentation by participants | |
| Around 11:00 | Coffee Break | |
| 12:10-12:30 | 15. Wrap up and Closing | |
| 12:30-14:00 | Lunch | |
| 14:00-18:30 | Technical Tour | |

## List of participants

**Bangladesh**

Ms Mossammat Ayesha Khatun
Deputy Director
Bangladesh Meteorological Department
Meteorological Complex, Agargaon, Dhaka-1207
Bangladesh
Tel.: +88-02-9135742 / +88-02-9141437
Fax: +88-02-8118230
E-mail: ayeshabmd@gmail.com

**Cambodia**

Mr Monichoth So Im
Deputy Director
Department of Meteorology
Ministry of Water Resources and Meteorology (MOWRAM),
#364 Monivong Bvld Chamkarmorn, Phnom Penh,
Kingdom of Cambodia
TEL: +855-11-274458
FAX: +855-23-213490
E-mail: monichoth@gmail.com

**Hong Kong, China**

Ms Man Sze Cheung
Experimental Officer
Hong Kong Observatory
134A Nathan Road, Kowloon
Hong Kong, China
TEL: +852-2926-3660
FAX: +852-2375-2645
E-mail: mscheung@hko.gov.hk

**Indonesia**

Mr Dadang Misbahudin
Head of Climate Early Warning Subdivision,
Agency for Meteorological Climatological and Geophysics in Indonesia (BMKG)
Jl. Angkasa 1, No.2, Kemayoran, Jakarta,
Indonesia. 10720
Republic of Indonesia
TEL: +62-21-654 5769
FAX: +62-21-654 5769
E-mail: dadangmsb@gmail.com

**Lao People's Democratic Republic**

Ms Khaemeuy Chao
Weather Forecaster
Department of Meteorology and Hydrology
Souphanouvong Avenue, Akart Village
Sikhottabong, District Vientiane Capital
Lao People's Democratic Republic
TEL: +856 21 215010, 263657
FAX: +856 21 223446, 520038
E-mail: khaemeuy@gmail.com,
dmhvte@etllao.com

**Malaysia**

Mr Nursalleh K Chang
Senior Assistant Director of Research and Technical Development
Malaysian Meteorological Department
Jalan Sultan, 46667 Petaling Jaya, Selangor
Malaysia
TEL: +60 379542146
FAX: +60 379540576
E-mail: nursalleh@met.gov.my

**Mongolia**

Dr Dulamsuren Dashkhuu (Ms)
Researcher
Climate Research Section
Information and Research Institute of Meteorology Hydrology and Environment (IRIMHE),
Juulchny gudamj-5, Chingeltei district,
Ulaanbaatar 15160
Mongolia
TEL: +976-88009788
E-mail: dumacn7803@yahoo.com

**Myanmar**

Ms Pa Pa Moe
Staff Officer
Department of Meteorology
No.5, Ministry of Transport and Communications
Myanmar
TEL: +95 067 441032
FAX: +95 067 411449
E-mail: papamoe187@gmail.com
dg.dmh1@gmail.com

**Pakistan**
Mr Muhammad Javaid Iqbal
Assistant Meteorologist,
Pakistan Meteorological Department
Meteorological Office, Allama Iqbal International Airport, Lahore
Islamic Republic of Pakistan
TEL: +92-42-99240403
FAX: +92-42-99240403
E-mail: javaid_met@yahoo.com

**Philippines**
Ms Ger Anne Marie Wales Duran
Weather Observer 1
Philippine Atmospheric, Geophysical and Astronomical Services Administration (PAGASA)
Science Garden Complex, Agham Rd. Diliman, Quezon City.
Republic of the Philippines
TEL: +632-434-0955
FAX: +632-434-0955
E-mail: marielduran25@gmail.com

**Singapore**
Mr Zheng Kaiyuan
Meteorologist
Weather Services Department
Meteorological Service Singapore
P.O. Box 8 Singapore Changi Airport, PTB II
Singapore
TEL: 65-6542-5059
FAX: 65-6545-7192
E-mail: Zheng_kaiyuan@nea.gov.sg

**Sri Lanka**
Ms I Mudiyanselage Shiromani Priyanthika Jayawardena
Deputy Director
Department of Meteorology
383, Bauddhaloka Mawatha, Colombo 07
Sri Lanka
TEL: +94 112676259
+94 714398874
FAX: +94 112698311
E-mail: shirojaya2000@yahoo.com,
shiro1010@gmail.com

**Thailand**
Ms Yuwadee Suwanmanee
Meteorologist
Thai Meteorological Department
4353 Sukhumvit Road, Bangna,
Bangkok 10260
Kingdom of Thailand
TEL: +662 3991423
FAX: +662 3838827
E-mail: yuwadee@tmd.go.th

**Viet Nam**
Mr Tran Quang Nang
Forecaster,
National Center for Hydro-Meteorological Forecasting (NCHMF),
No 4 Dang Thai Than, Hoan Kiem district, Hanoi
Viet Nam
TEL: +84 438247002
FAX: +84 438254278
E-mail: trannang030984@gmail.com

# “Introduction to Climatology” for experts on climate services

# “Introduction to Climatology” for experts on climate services

Shuhei MAEDA (smaeda@mri-jma.go.jp)
Climate Research Department, Meteorological Research Institute (MRI/JMA)
1-1 Nagamine, Tsukuba, 305-0052, JAPAN

## 1. Climate and Climate system

According to WMO website, “on the simplest level the weather is what is happening to the atmosphere at any given time. Climate, in a narrow sense, can be considered as the ‘average weather,’ or in a more scientifically accurate way, it can be defined as ‘the statistical description in terms of the mean and variability of relevant quantities over a period of time.’” Although climate is the synthesis of the weather, climate is not maintained only by atmosphere itself but is formed in the interactions among many components of the Earth. This system is named as a climate system. The global climate system consists of atmosphere including its composition and circulation, the ocean, hydrosphere, land surface, biosphere, snow and ice, solar and volcanic activities (Fig.1). These components interact on various spatial and temporal scales through the exchanges of heat, momentum, radiation, water and other materials.

The purpose of the lecture is to know how climate is formed and its variability is caused. In the lecture, anthropogenic “climate change” defined by United Nations Framework Convention on Climate Change (UNFCCC) is not explicitly included. As for “climate change”, please refer to other text books or the item 5 of the TCC seminar text book in 2014 written by Dr. Ose.

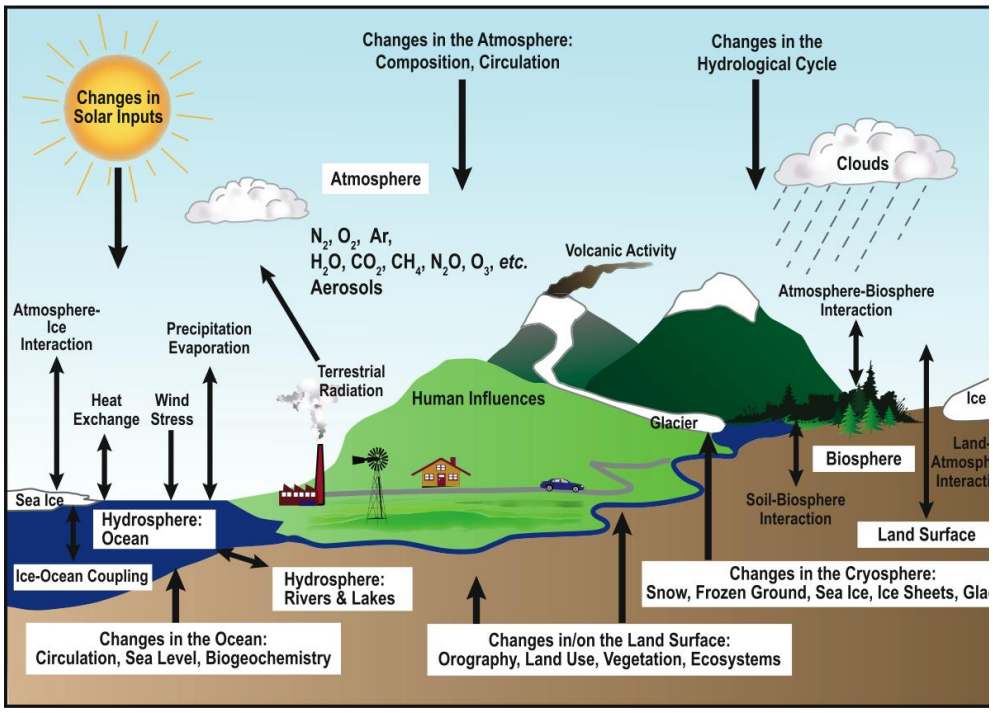


**Figure 1 Schematic view of the components of the climate system, there processes and interactions. From IPCC (2007).**

## 2. Global mean temperature and Radiative balance

Global mean temperature of planets, which is the temperature "observed from space", is estimated by global radiation balance between absorbed solar radiation and terrestrial emission from the planet. Incoming solar radiation is reflected back to space by a fraction of the planetary albedo. For the Earth, the observed mean ground temperature (15°C) is warmer by 34°C than the estimated temperature (-19°C). The reason is suggested by comparing other planet cases. The mean ground temperature for Mars with thin atmosphere is warmer only by 1°C than the estimated temperature. For Venus with thick atmosphere, the difference is 503°C. Radiative absorption by greenhouse gas in atmosphere is an important factor to determine mean ground temperature as well as planetary albedo.

The Earth's atmosphere has different characteristics for shortwave and longwave radiations (Fig.2). It is transparent (about 50%) for shortwave radiative flux from the sun as an approximation except for the reflection due to clouds (about 20%). On the other hand, the longwave radiation flux emitted from the Earth's ground is absorbed (about 90%) once in the atmosphere approximately and then mostly emitted back to the ground (greenhouse effect). Upper cold atmosphere and clouds emit less longwave flux to space than the ground emits. As a net, surface ground is heated by shortwave radiation from the sun, and atmosphere is cooled by longwave emission to space. The vertical contrast of the heating between ground and atmosphere creates thermal instability, which is compensated by vertical transport processes of sensible and latent heat energy due to turbulences, convections and waves.

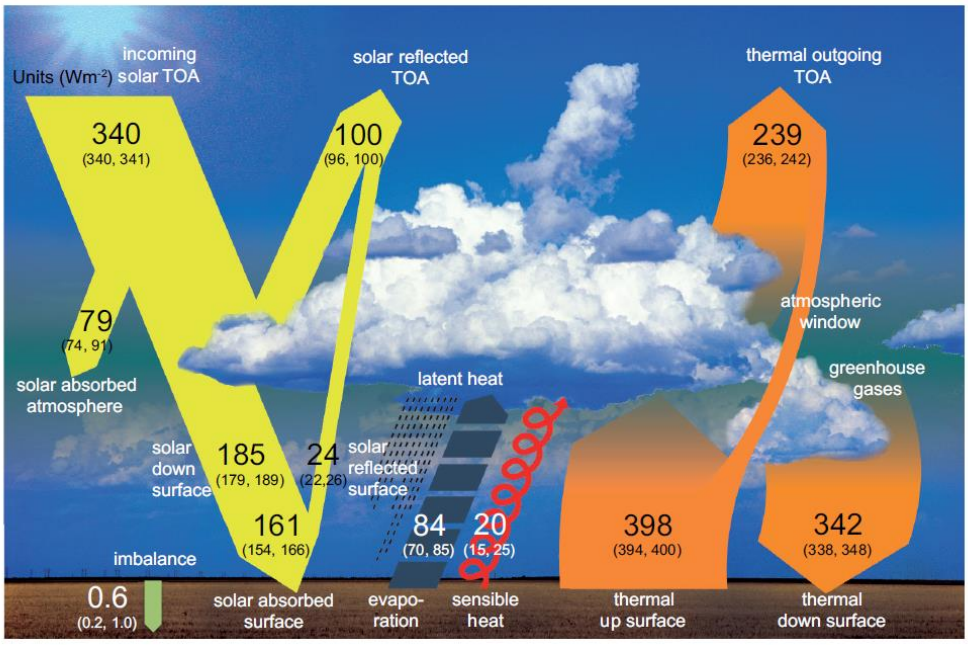


**Figure 2 Schematic diagram of the global mean energy balance of the Earth. Numbers indicate best estimates for the magnitudes of the globally averaged energy balance components together with their uncertainty ranges, representing present day climate conditions at the beginning of the twenty first century. Units W/m$^2$. From IPCC (2014).**

## 3. Annual mean circulation and Horizontal heating contrast

Longitudinal contrast of radiative heating is created between day and night (Fig.3). But, generally, as compared with the annual cycle, the diurnal heating contrast does not produce significant temperature differences between day and night and related global circulations because a relaxation time to a radiative equilibrium is estimated as 30 days for the Earth (James, 1995), which is much longer than a day scale. Latitudinal heating contrast on the Earth is created on seasonal time-scale by the different incoming shortwave radiation between near the poles and the tropics (Fig.3). Local surface temperature determining outgoing longwave radiation is not adjusted instantly enough to compensate for the shortwave radiation contrast. A part of absorbed radiative energy in low latitudes is transported poleward by meridional circulations and waves in atmosphere and ocean, and these heat transports keep high-latitudes warmer than the radiative equilibrium.

Poleward/equatorward air motions form westerly/easterly wind in the upper/lower subtropics (Fig.4) through Coriolis force due to the rotation of the Earth (or the angular momentum conservation about the Earth's rotation axis). Extra-tropical waves are also responsible for creating mid- to high latitude's westerly jets.

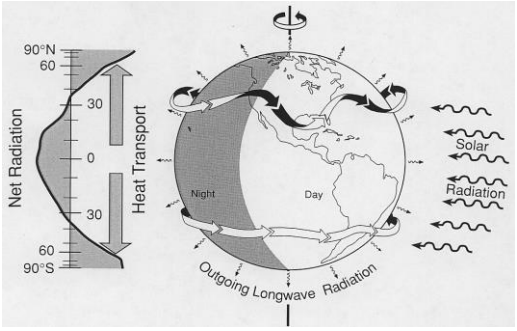


**Figure 3 Horizontal radiative imbalance and energy transport by the atmosphere and ocean. From IPCC (1995).**

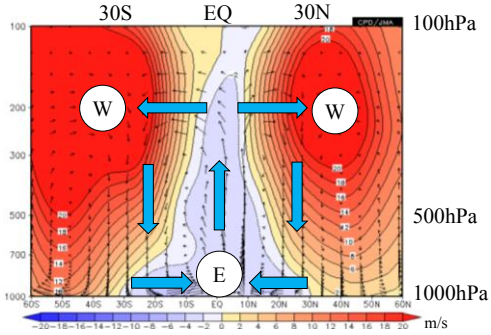


**Figure 4 Annual and zonal mean wind. Shade: zonal wind, and arrow: meridional and vertical wind.**

## 4. Seasonal change and Heat capacity

Seasonal change is definitely produced by the seasonally changing solar incidence with its maxima at the South Pole in December and at the North Pole in June. However, zonally averaged features of temperature are not drastically changed in the troposphere (lower than about 100hPa) through the whole year, hot tropics and cold poles (Fig.5). This fact is attributed to basically unchanged distribution of sea surface temperature (SST) due to large heat capacity of the oceans; in the Earth, heat capacity of the ocean is about 1,000 times of that of the atmosphere. SSTs roughly determine the location of deep cumulus occurrences, which leads to vertical energy mixing in the troposphere and drives global circulations (Webster, 1994). Stratospheric climate above 100hPa varies following the seasonal march of the sun (Fig.5)

because of the seasonal change of ozone-related shortwave heating and small heat capacity of thin stratospheric atmosphere; cold around a winter pole, warm around a summer pole. Atmospheric circulations also contribute to the stratospheric climate; a cold tropopause in the tropics is steadily created by upward motion.

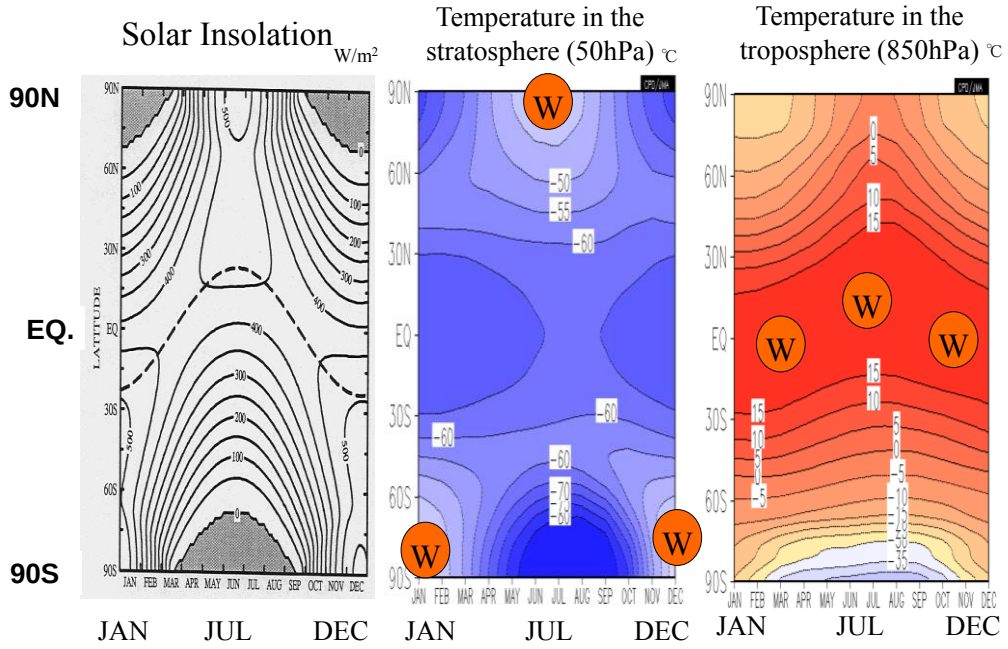


**Figure 5 Seasonal change of (left) solar insolation, zonally averaged temperature (middle) at 50hPa and (right) at 850hPa. The figure for solar insolation is from IPCC (1995).**

Heat capacity of land surface is small as compared with that of the oceans. Surface air temperature over the northern continents is much higher than SSTs at the same latitudes in the northern summer (especially in daytime) and much colder in the northern winter (Fig.6). The large contrasts of surface air temperature between continents and the oceans add a significant feature to regional seasonal changes of rainfall and wind around the continents in low and mid-latitudes, which is named as monsoon. A concentrated subtropical rainfall forms a typical summer monsoon system consisting of an upper-level anti-cyclonic circulation, a monsoon trough, a low-level jet, a subtropical rainfall band expanding north eastward (south eastward) and extensive downward motions causing dry region in the north westward (south westward) area of the Northern (Southern) Hemisphere (Rodwell and Hoskins, 1996), as shown in the Asian region of Fig.6 and Fig. 7.

**Jan-Jul contrast of surface temperature/precipitation**

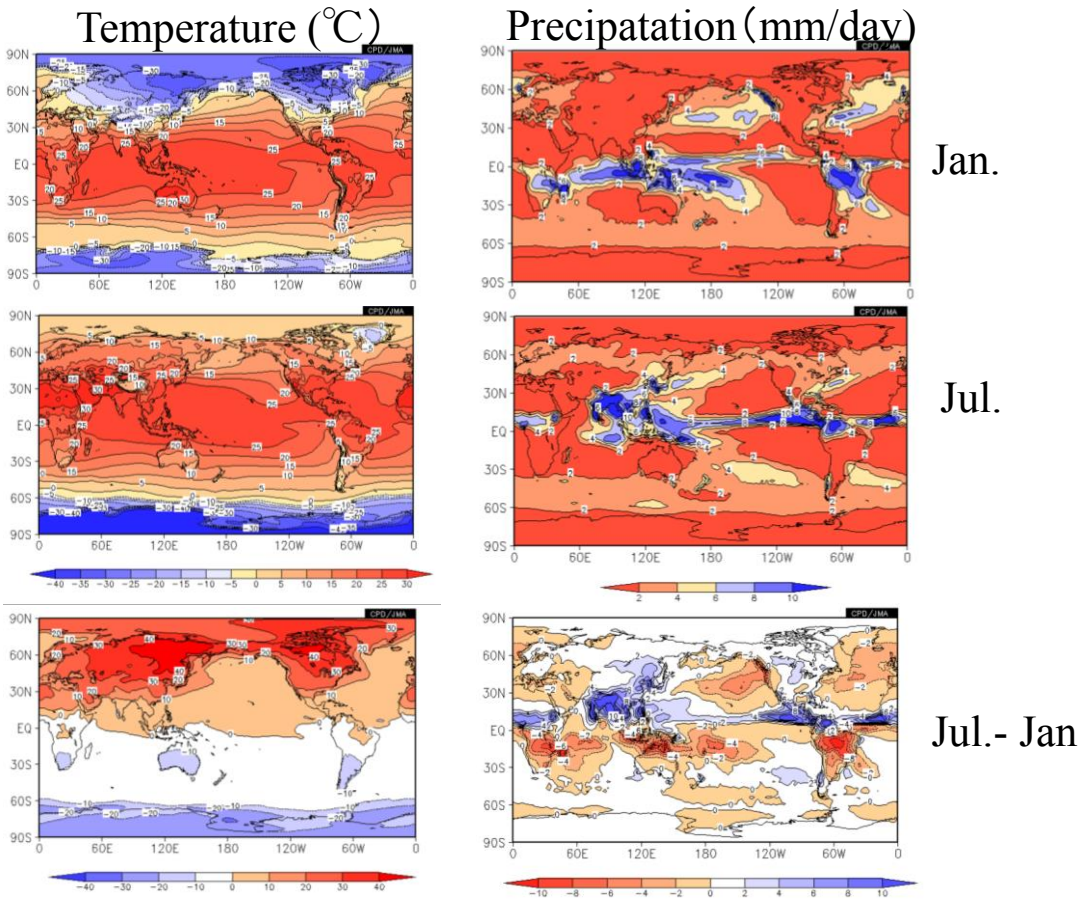


**Figure 6 (Left) surface are temperature and (right) precipitation in (upper) January, (middle) July, and (bottom) deference between the two months.**

# Northern Summer Monsoon circulation

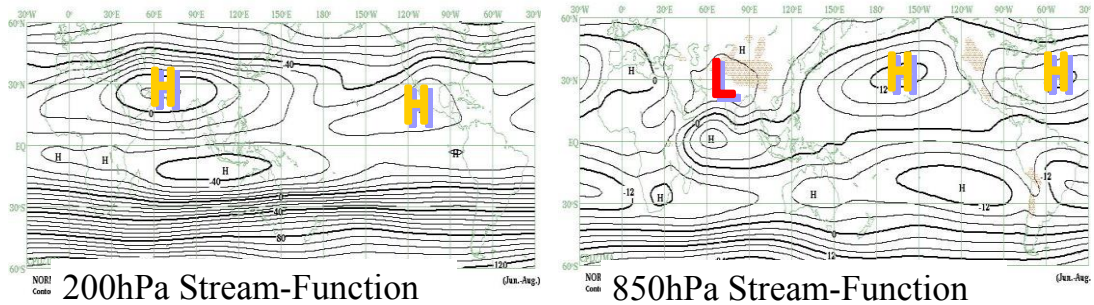


**Figure 7 (Left) 200hPa stream function and (right) 850hPa stream function in JJA.**

Mountains have also impact on seasonal changes in local climate through thermal and dynamical processes. A good way to understand climate system is to modify or remove some elements of the climate system (Fig. 1). It is not easy to modify a real climate system of the Earth by changing the Earth orbit or removing mountains. Instead, we can easily modify virtual climate systems simulated numerically in climate models based on physics and other fundamental sciences. From the comparison between with/without mountain model experiments (Fig. 8), we can see that mountains would be responsible for the real world climate of humid summer and somewhat cold winter in the eastern parts of the continents.

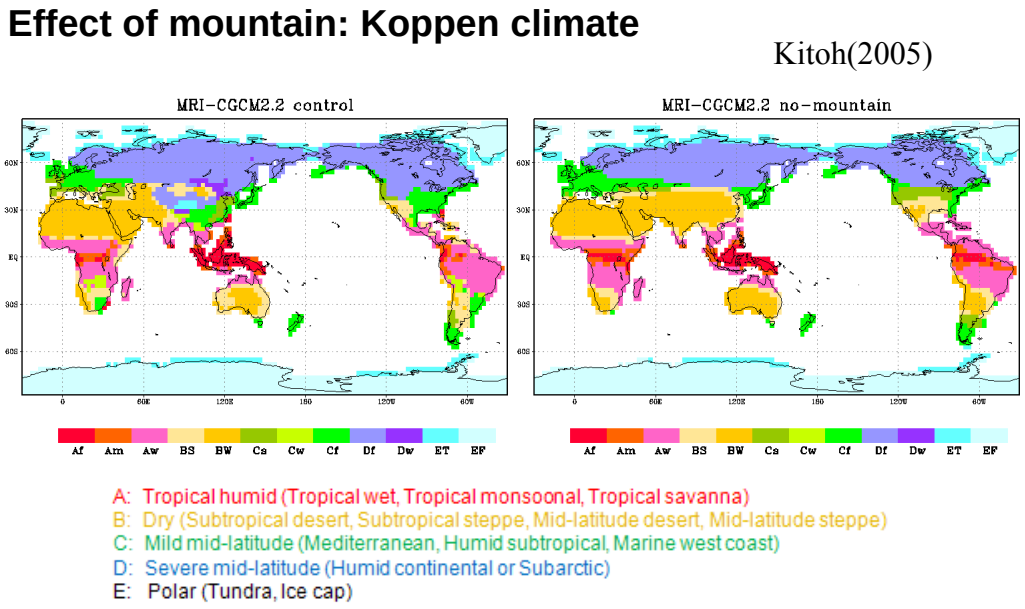


**Figure 8 Köppen climate maps simulated by a climate model (left) with mountains and (right) without mountains. From Kitoh (2005) in Japanese.**

## 6. Intra-seasonal to Interannual variability

Climate varies naturally with time. Atmosphere itself includes internal instability mechanisms, typically the baroclinic instability around the extratropical westerly jets, so that it may be considered as chaotic or unpredictable beyond a few weeks. However, some atmospheric low-frequency (>10days) teleconnections are analyzed such as wave patterns along the westerly jet waveguides and other ones from the northern mid-latitudes across the equatorial westerlies (Fig. 9), which are consistent with the Rossby-wave propagation theory. Also, teleconnections of another type are analyzed such as meridional displacements of the westerly jet (Fig.10), which are maintained by the wave-mean flow interaction (Vallis, 2006). Numerical ensemble predictions from many disturbed atmospheric initials are a reasonable tool to capture mean weathers in next few weeks.

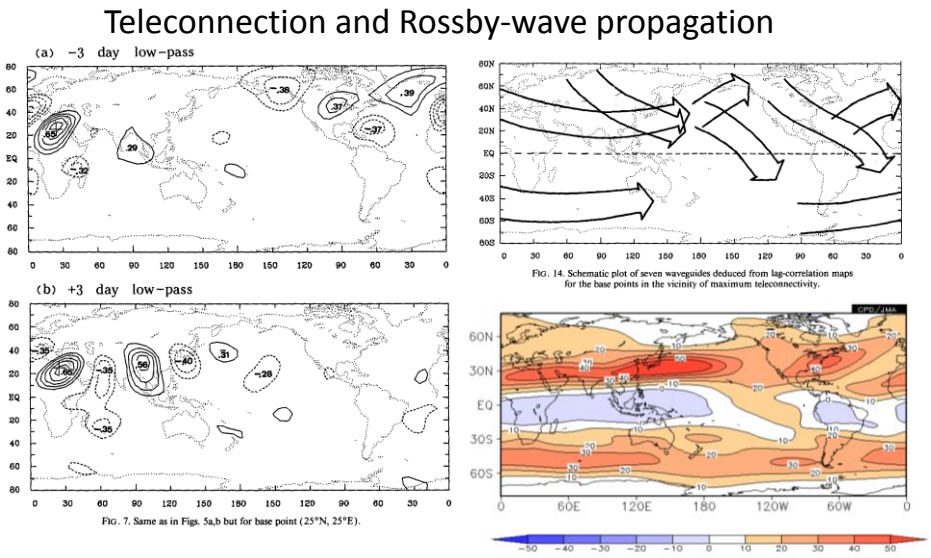


**Figure 9 (Left) a teleconnection pattern of 250hPa stream function in boreal winter, (upper-right) various propagations of Rossby-wave and (lower-right) 250hPa climatological zonal wind in DJF. Left and upper-right panels are from Hsu and Lin (1992).**

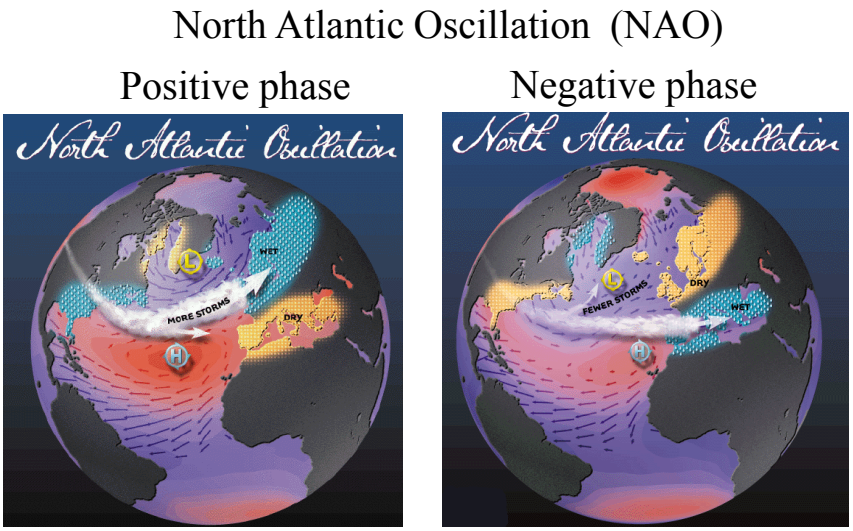


From http://www.ldeo.columbia.edu

**Figure 10 (Left) positive and (right) negative phase of North Atlantic Oscillation (NAO). NAO is one of teleconnections with meridional displacements of the westerly jet. Panels are from http//www.ldeo.columbia.edu.**

In the tropics, some peaks in spatial and temporal power-spectrums, indicating organized atmospheric variability coupled with convective activity, are imbedded in red noise backgrounds. Variability of outgoing longwave radiation (OLR) associated with equatorial waves, such as Kelvin waves, equatorial Rossby waves (ER) and mixed Rossby-Gravity waves (MRG), can be detected, in Fig. 11.

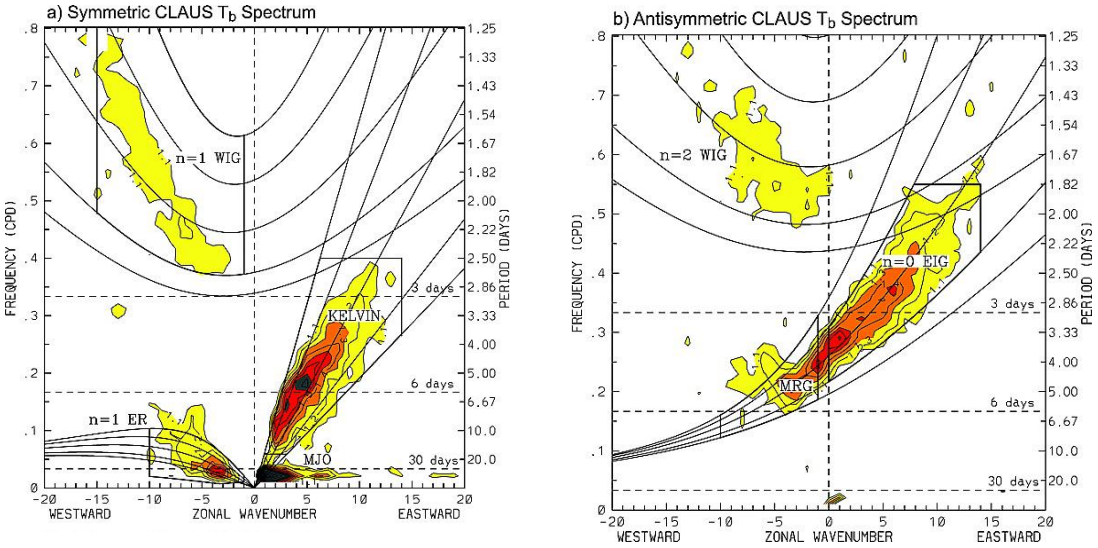


Wave number–frequency power spectrum of the (a) symmetric and (b) antisymmetric component of Cloud Archive User Services (CLAUS) $T_b$ for July 1983 to June 2005, summed from 15° N to 15° S, plotted as the ratio between raw $T_b$ power and the power in a smoothed red noise background spectrum (see WK99 for details). Contour interval is 0.1, and contours and shading begin at 1.1, where the signal is significant at greater than the 95% level. Dispersion curves for the Kelvin, $n = 1$ equatorial Rossby (ER), $n = 1$ and $n = 2$ westward inertio-gravity (WIG), $n = 0$ eastward inertio-gravity (EIG), and mixed Rossby-gravity (MRG) waves are plotted for equivalent depths of 8, 12, 25, 50, and 90 m. Heavy solid boxes represents regions of wave number–frequency filtering

**Figure 11 Spatial and temporal power-spectrums in the tropics of (left) symmetric and (right) asymmetric OLR variability about the equator. (From Kiladis et al. 2009).**

The Madden-Julian Oscillation (MJO) is an eastward-moving oscillation of surface pressure, precipitation and winds along the equator with the period of 30-60 days and planetary scale wavenumbers (Fig. 12). Monitoring MJO or watching OLR and velocity potential anomalies may be very helpful for intra-seasonal prediction in the tropics to the subtropics and even in the mid-latitudes (Fig. 12). Improvement of MJO prediction skill is one of key topics for operational numerical prediction centers in the world.

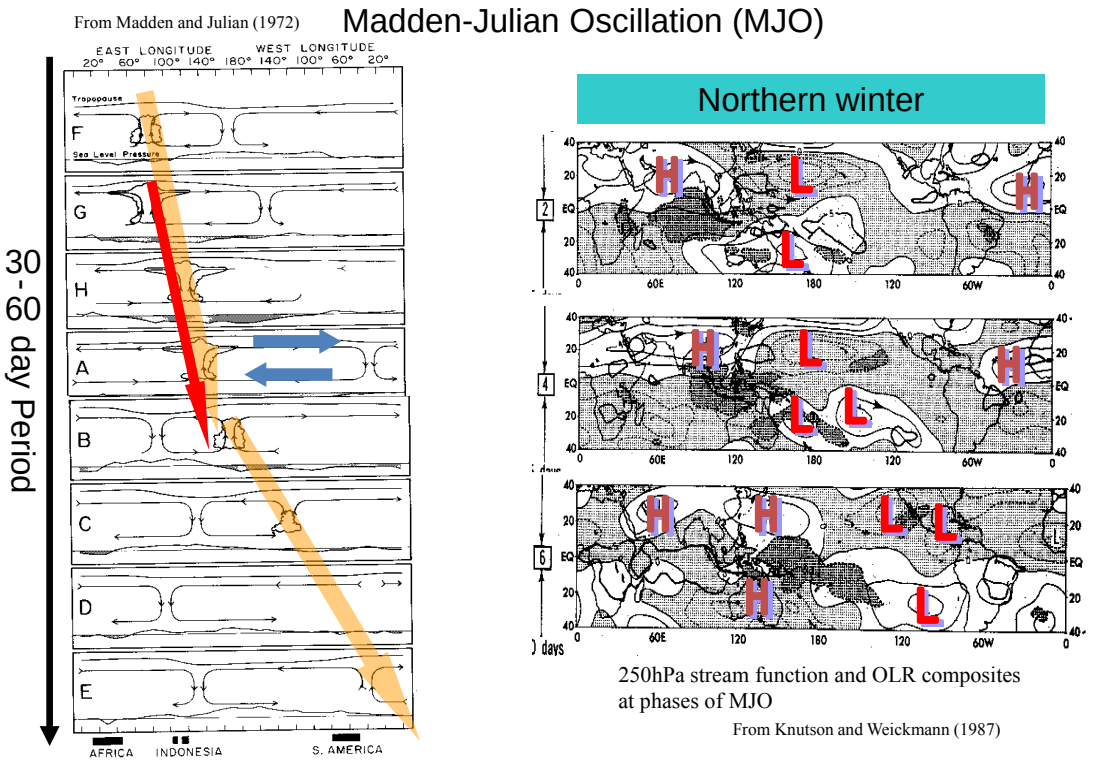


**Figure 12 (Left) schematic time-sequence of Madden-Julian Oscillation (MJO) along the equator (from Madden and Julian, 1972). (Right) composite maps of OLR and 250hPa stream function anomaly at MJO phases (from Knutson and Weickmann 1987).**

Atmosphere-ocean interactions are able to produce longer time-scale natural variability in atmosphere with periods beyond months up to several and decadal years. A typical example is ENSO (El Niño / Southern Oscillation) with the period of 2-7 years, which is the most dominant interannual climate variability in the earth climate system and has huge sociological and economic impacts globally. El Niño events themselves, and related surface air temperature and precipitation anomalies are predicted successfully on seasonal to inter-annual scales (Fig.13). The SST anomalies with El Niño tend to keep seasonally steady precipitation (heating) anomalies over the equatorial central Pacific. The response of the upper and lower-level tropical atmosphere to these steady heating anomalies can be explained based on forced equatorial waves or the Gill-pattern (or Matsuno-Gill pattern) (Fig. 14). These anomalous steady heating in the tropics forces stationary Rossby waves which propagate to mid-latitudes, and tends to cause teleconnection patterns such as the Pacific North America (PNA) pattern and the Western Pacific (WP) pattern.

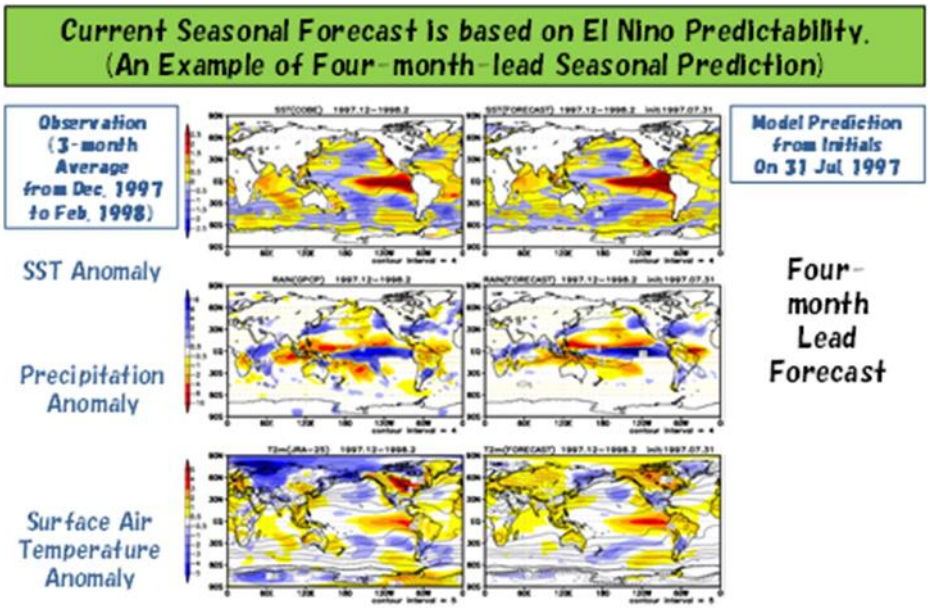


Figure 13 (Left) observed SST, precipitation and surface air temperature anomalies for DJF 1997-98. (Right) the same except for four-month lead prediction.

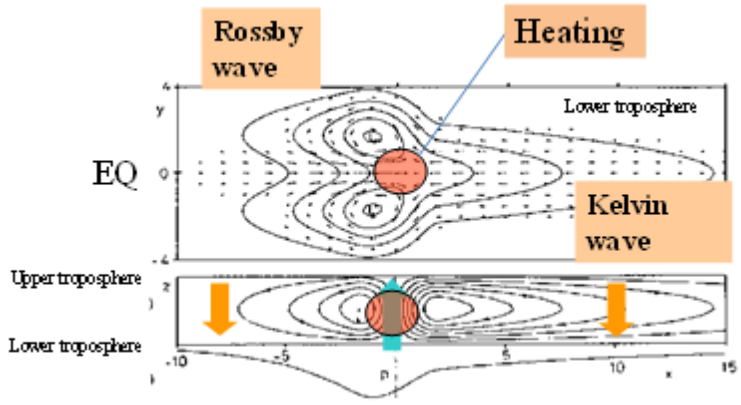


**Figure 14 Tropical atmospheric responses to equatorially symmetric heating anomalies. (from Gill 1980).**

Recently, terms of “El Niño Modoki” or “Central Pacific (CP)-El Niño” are used to distinguish them from normal El Niño events or Eastern Pacific (EP)-El Niño. They consist of the equatorial Pacific phenomena with warm SST anomalies and enhanced precipitation in the central Pacific, and cold SST anomalies and suppressed precipitation in the eastern Pacific, on contrast. The remote effect of El Niño during the mature stage is stored in the Indian Ocean capacity and still influential to the Indo-western Pacific climate even during summer following the ENSO (Fig.15). A dipole mode with an east-west SST anomaly contrast sometimes occurs around September and October in the tropical Indian Ocean, which is at least partially independent from ENSO events (Fig. 16). Occurrence of this mode affects climate over various regions including tropical eastern Africa and the maritime continent.

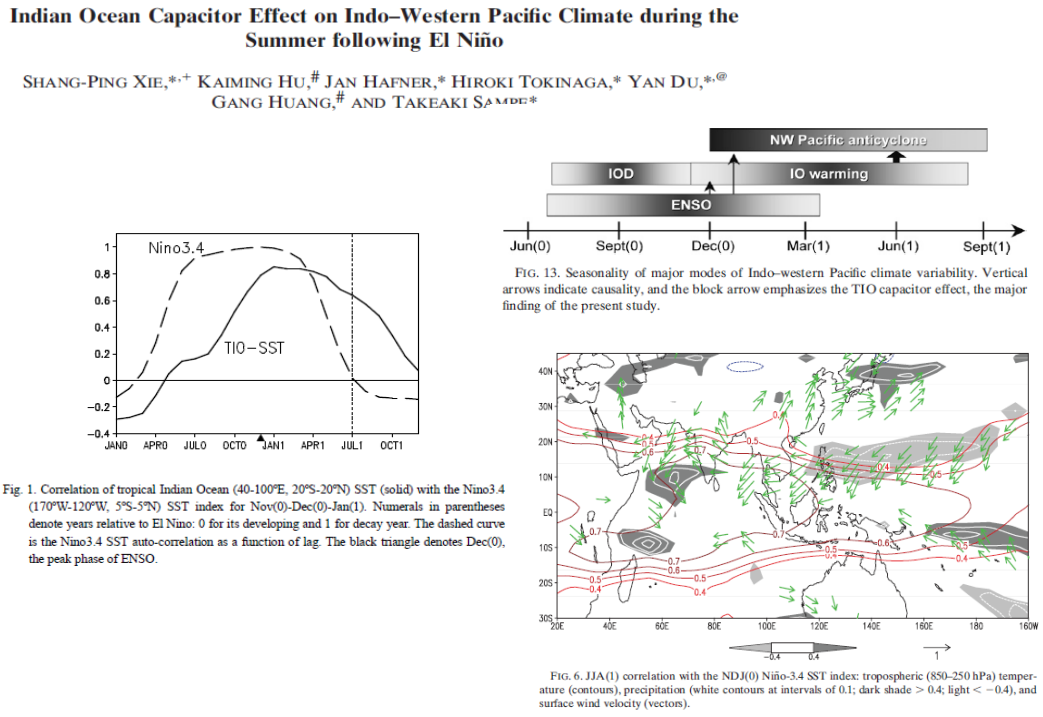


Fig. 1. Correlation of tropical Indian Ocean (40-100°E, 20°S-20°N) SST (solid) with the Nino3.4 (170°W-120°W, 5°S-5°N) SST index for Nov(0)-Dec(0)-Jan(1). Numerals in parentheses denote years relative to El Nino: 0 for its developing and 1 for decay year. The dashed curve is the Nino3.4 SST auto-correlation as a function of lag. The black triangle denotes Dec(0), the peak phase of ENSO.

FIG. 13. Seasonality of major modes of Indo–western Pacific climate variability. Vertical arrows indicate causality, and the block arrow emphasizes the TIO capacitor effect, the major finding of the present study.

FIG. 6. JJA(1) correlation with the NDJ(0) Niño-3.4 SST index: tropospheric (850–250 hPa) temperature (contours), precipitation (white contours at intervals of 0.1; dark shade > 0.4; light < −0.4), and surface wind velocity (vectors).

**Figure 15 Indian Ocean capacitor effect. (Left) lagged correlation of tropical Indian Ocean SST with Nino 3.4 SST for NDJ. (Upper-right) seasonality of major modes. (Lower-right) correlation of the NDJ Nino3.4 SST with the following JJA climate. From Xie et al. (2009).**

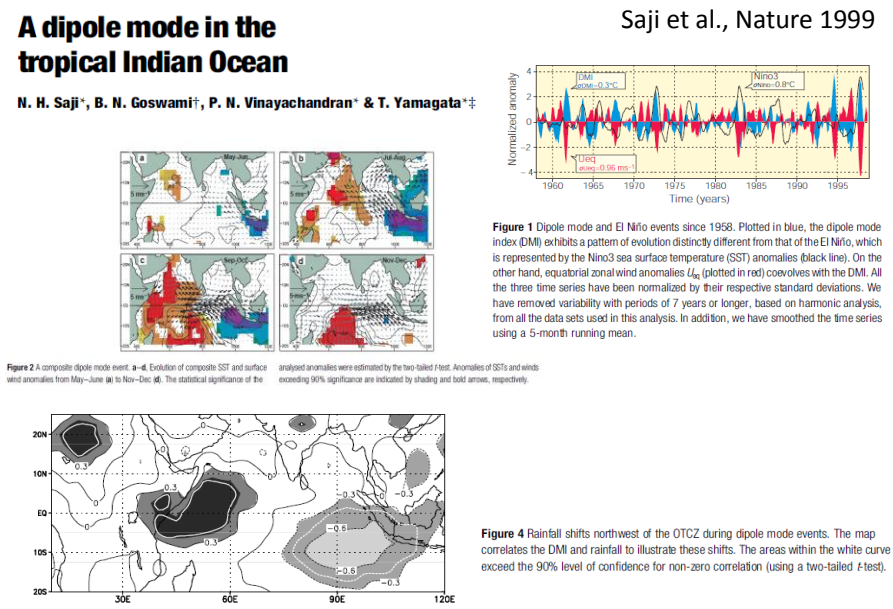


**Figure 16 A dipole mode in the tropical Indian Ocean. (Upper-left) time-evolution of the dipole mode SST anomaly, (lower-left) rainfall shift during the dipole mode, (right) historical records for dipole mode and El Niño events. From Saji et al. (1999).**

## 7. Decadal variability

Decadal variability and climate change involve feedbacks from other elements of the climate system. Changes of vegetation and soil moisture amplify the dramatic drying trend in 1980's in Sahel region, which is basically forced by a southward precipitation shift of the Inter-tropical Convergence Zone due to cooler/warmer SST anomaly in the northern/southern Atlantic Ocean (Fig. 17).

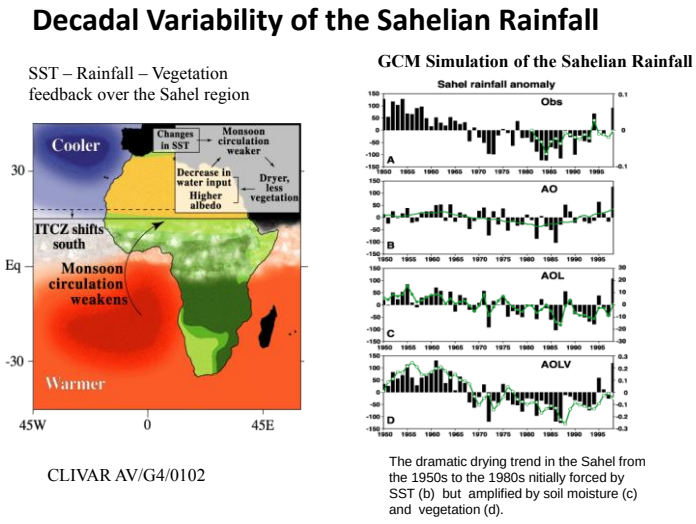


**Figure 17 Decadal variability of the Sahel Rainfall. (Left) a possible mechanism, (Right) observed historical Sahel rainfall anomaly and GCM simulations . From Zeng et al. 1999.**

Decadal variabilities are also found in SST anomaly from the North Pacific to the tropics (Fig. 18) which is named Pacific Decadal Oscillation (PDO) or Interdecadal Pacific Oscillation (IPO). A possible mechanism of PDO is the subduction hypothesis; high latitudes' cold surface water is subducted in the North Pacific and flows into the subtropical deeper ocean along the surfaces of constant density, then emerges again to the surface of the equatorial Pacific by upwelling. This is consistent with the analysis showing that the decadal SST variability in the central North Pacific spreads into the deep ocean. PDO has impact on ENSO characteristics and regional climate. Several studies indicated that the negative phase of PDO played the major role in the slowdown of the global averaged surface air temperature raise in recent years (Meehl, 2015).

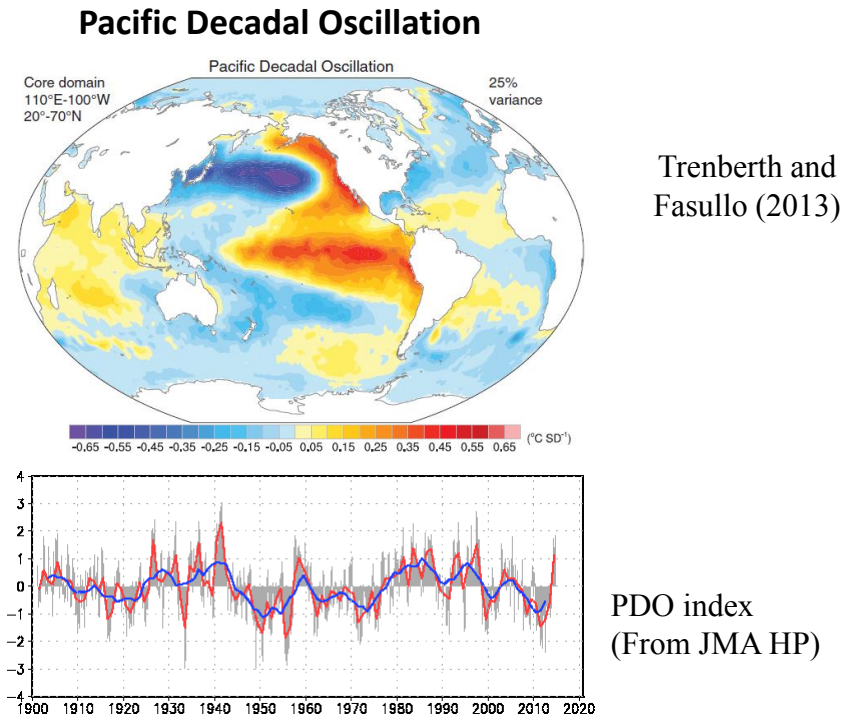


**Figure 18 (Upper) SST anomaly pattern in the positive phase of Pacific Decadal Oscillation (PDO)(from Trenberth and Fasullo, 2013) and (lower) PDO index (the latest index is available from http://ds.data.jma.go.jp/tcc/tcc/products/elnino/decadal/pdo.html).**

## 8. Summary

Unusual weather and climate are attributed to unusual atmospheric flows, storms and convective disturbance. Diagnostic analysis shows that those disturbances are often related to atmospheric intrinsic waves and phenomena. However, atmospheric environment is maintained and influenced by other elements consisting of the climate system. Sometimes, and unusual and steady convective activity is connected to long-term SST anomalies related to ocean variability. Numerical ensemble simulations starting from many disturbed atmospheric and oceanic initials are a reasonable tool to capture the mean state of weathers and climate in a timescale from

weeks to seasons. Radiative processes including longwave absorption by greenhouse gases and shortwave reflection by snow, ice, clouds and aerosols determine the local Earth's ground temperature. The distribution of ground temperature is influential to vertical and horizontal atmospheric and oceanic stabilities, the amount of water vapor and the speed of water cycle. Then, those can affect atmospheric and oceanic flows, the features of storms and convections and eventually our daily lives. Therefore, we need to continue careful watches and diagnostics for global and local climate systems (Fig.1), as well as its prediction.

## References


Deser, C., M. A. Alexander and M. S. Timlin, 1996: Upper-ocean thermal variations in the North Pacific during 1970-1991. *J. Climate*, **9**, 1840-1855.

Gill, A. E., 1980: Some simple solutions for heat-induced tropical circulation. *Quart. J. Meteor. Soc.*,**106**, 447-462.

Hsu, H.-H., and S.-H. Lin, 1992: Global teleconnections in the 250-mb streamfunction field during the Northern Hemisphere winter. *Mon. Wea. Rev.*, **120**, 1169-1190.

IPCC Second Assessment Report (SAR) Climate Change 1995: The Science of Climate Change.

IPCC Fourth Assessment Report (AR4) Climate Change 2007: The Physical Science Basis.

IPCC Fifth Assessment Report (AR5) Climate Change 2014: The Physical Science Basis.

Kiladis, G. N., M. C. Wheeler, P. T. Haertel, K. H. Straub, and P. E. Roundy, 2009: Convectively coupled equatorial waves. Rev. Geophys., 47, RG2003, doi:10.1029/2008RG000266.

Kitoh, A., 2005: Climate model simulation on the role of mountain uplift on Asian monsoon. The Geological Society of Japan, 111, XIX.

Knutson, T. R. and K. M. Weickmann, 1987: 30-60 day atmospheric oscillations: composite life cycles of convection and circulation anomalies. *Monthly Wea. Rev.* **115**, 1407-1436.

Madden, R. A. and P. R. Julian, 1994: Observations of the 40–50-day tropical oscillation—A review, *Monthly Wea. Rev.*, **122**, 814–37.

Meehl G. A., 2015: Deacadal climate variability and the early-2000s hiatus. US CLIVAR, 13, No.3, 1-6.

Rodwell, M.J. and B. I Hoskins, 1996: Monsoons and the dynamics of deserts. *Q. J. R. Meteor. Soc.*, **122**, 1385-1404.

Saji, N. H., B. N. Goswami, P. N. Vinayachandran and T. Yamagata, 2009: A dipole mode in the tropical Indian Ocean. *Nature*, **401**, 360-363.

Trenberth, K.E and J. T. Fasllo, 2013: An apparent hiatus in global warming?. Earth's Future 1, 19-32.

Webster, P. J., 1994: The role of hydrological processes in ocean-atmosphere interactions, *Review of Geophysics*, **32**,427-476.

Weng, H., K. Ashok, S. Behera, S. A. Rao and T. Yamagata, 2007: Impacts of recent El Nino Modoki on dry/wet conditions in the Pacific rim during boreal summer. *Clim Dyn.*, **29**, 113-129.

Xie, S.-P., K. Hu, J. Hafner, H. Tokinaga, Y. Du, G. Huang and T. Sampe, 2009: Indian Oceancapacitor effect on Indo-western Pacific climate during the summer following El Niño. *J. Climate*, **22**, 730-747.

Zeng, N., J. D. Neelin, K.-M. Lau and C. J. Tucker, 1999: Enhancement of interdecadal climate variability in the Sahel by vegetation interaction. *Science*, **286**, 1537-1540.

### Textbooks

James, I. N., 1995: Introduction to Circulating Atmospheres. Cambridge University Press, 422pp.

Trenberth, K.E.(ed.), 1992: Climate System Modeling. Cambridge University Press, 788pp.

Valls G. K., 2006:Atmospheric and oceanic fluid dynamics. Cambridge University Press, 7454pp.

Wallace, J.M. and P. V. Hobbs, 2006: Atmospheric Science. Academic Press, 483pp.

# Interannual to decadal variability in the tropical oceans

# Interannual to decadal variability in the tropical oceans

Tamaki YASUDA
Climate Prediction Division, Japan Meteorological Agency (JMA)

## 1. Introduction

Tropical oceans play major roles in global climate variability. Atmosphere-ocean coupled phenomena in the tropical oceans induce global atmospheric and oceanic circulations that affect regional climate variability. On the interannual time scale, El Niño/Southern Oscillation (ENSO) of the tropical Pacific is known as a typical example of such phenomena. Recently, terms of "El Niño Modoki" or "Central Pacific (CP) El Niño" are used to distinguish them from canonical El Niño events or Eastern Pacific (EP) El Niño. Variability of the tropical Indian Ocean such as Indian Ocean Basin Wide (IOBW) and Indian Ocean Dipole (IOD) modes also impacts on global climate, especially the Asian and African climate. Beyond ENSO time scale, decadal variability such as the Pacific Decadal Oscillation (PDO) is associated with ENSO and global warming and related global climate. In this lecture, climate variability in tropical oceans on the interannual to decadal time scales are explained from the viewpoint of the oceanic variability.

## 2. El Niño/Southern Oscillation (ENSO)

Interannual variability in the Pacific is dominated by El Niño/Southern Oscillation (ENSO), which has its largest signature in the tropics. This phenomenon appears primarily to be the result of interactions between the tropical oceans and overlying atmosphere (Philander 1990), and thus produces sea surface temperature (SST) and heat content anomalies that are concentrated in the tropics.

El Niño (La Niña) event is a phenomenon that an area of warmer (cooler)-than-normal SST persists in the central and eastern parts of the equatorial Pacific for 6 to 18 months. Figure 1 shows SST distributions in December in normal years and El Niño years (2012 and 2015,

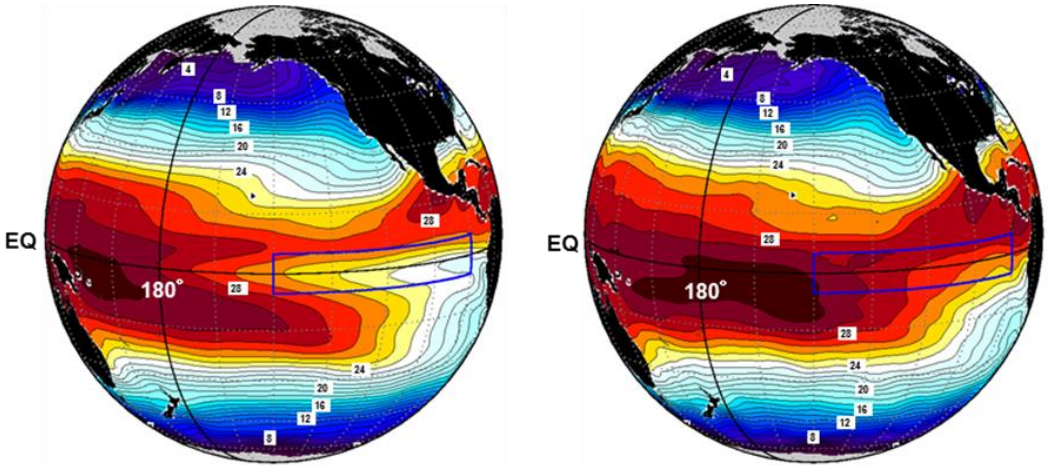


Figure 1 Monthly mean sea surface temperature in December in 2012 (normal year: left) and 2015 (El Niño year: right). Rectangle area indicates the El Niño monitoring region (NIÑO.3: 5°S-5°N, 150°-90°W).

respectively). In December 2015, waters warmer than normal are seen from around the date line to the west coast of Peru in the equatorial Pacific. During an El Niño event, the region of SST above 28˚C, which is related to active evaporate for the sea, extends eastward, and the precipitation area shifts eastward 6,000-12,000 km.

Figure 2 shows schematic diagrams of zonal sections of atmospheric and oceanic conditions along the equatorial Pacific during a normal period, an El Niño event and a La Niña event. During an El Niño event (bottom left panel), the trade wind is weaker than normal and surface warm water spreads further east than normal. SST pattern in December 2015 shown in the right of Figure 1 reveals this feature. The active convection area shifts eastward associated with this change in SST pattern. During a La Niña event (bottom right panel of Figure 2), atmospheric and oceanic conditions seen in the normal years are reinforced. Trade wind is stronger, atmospheric convection is more active in the western Pacific. More warm waters are accumulated in the western Pacific and more cold waters move upward in the eastern Pacific due to the stronger trade wind. In other words, El Niño and La Niña events are the large scale atmospheric-ocean coupled phenomena that changes in the zonal gradient of ocean temperature and Walker circulation due to zonal shift of active convection area are impact each other.

In the developing stage of ENSO, a positive feedback of atmosphere-ocean coupled interaction, i.e., Bjerknes feedback is an essential mechanism (Bjerknes, 1999). For mechanisms of the quasi-periodic oscillation of ENSO, two major theories, i.e., the delayed oscillator (Schopf and Suarez, 1988; Suarez and Schopf, 1988) and the recharge-discharge oscillator (Jin,

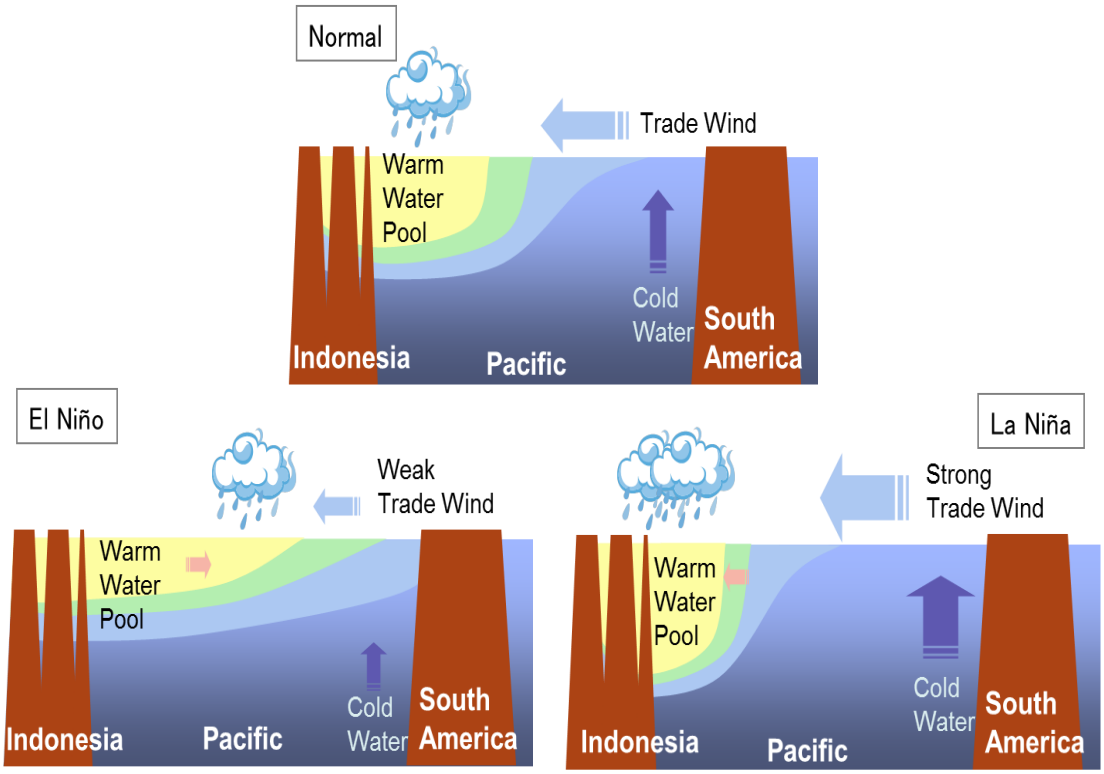


Figure 2 Schematic views of atmospheric and oceanic conditions in the equatorial Pacific during a normal condition (top), an El Niño event (bottom left), and a La Niña event (bottom right).

1997a, b) have been proposed. The delayed oscillator explains El Niño developing due to the downwelling Kelvin wave and Bjerknes feedback, and El Niño terminating due to upwelling Kelvin wave resulting from the westward propagating Rossby wave reflected at the western boundary (Figure 3). Recharge-discharge oscillator emphasizes the major role of the storage of equatorial heat and how that leads to a self-sustaining oscillation shown in Figure 4.

ENSO affect the global atmospheric circulation, and cause extreme weather events all over the world. Figure 5 shows schematic charts of typical anomaly patterns of surface temperature and precipitation for boreal summer and winter in past El Niño/La Niña events.

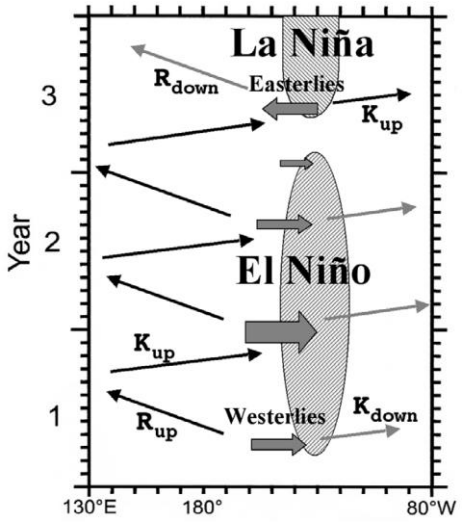


Figure 3 Schematic time-longitude diagram of the delayed oscillator theory for ENSO. From Wang and Picaut (2004).

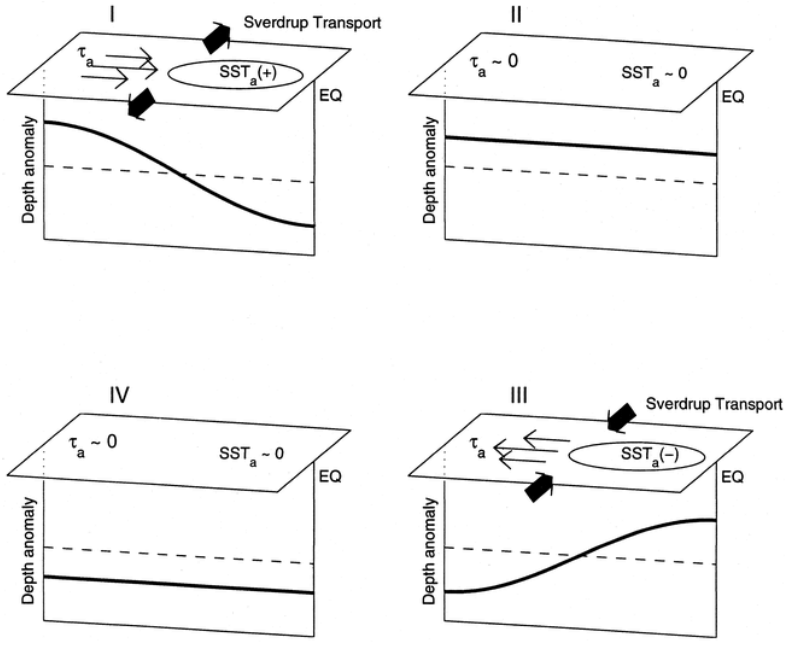


Figure 4 Idealized schematic of the El Niño-La Niña oscillation in recharge-discharge oscillator theory. Oscillation progresses clockwise around the panels following the roman numerals; panel I represents El Niño conditions, panel III indicates La Niña conditions. From Meinen and McPhaden (2000).

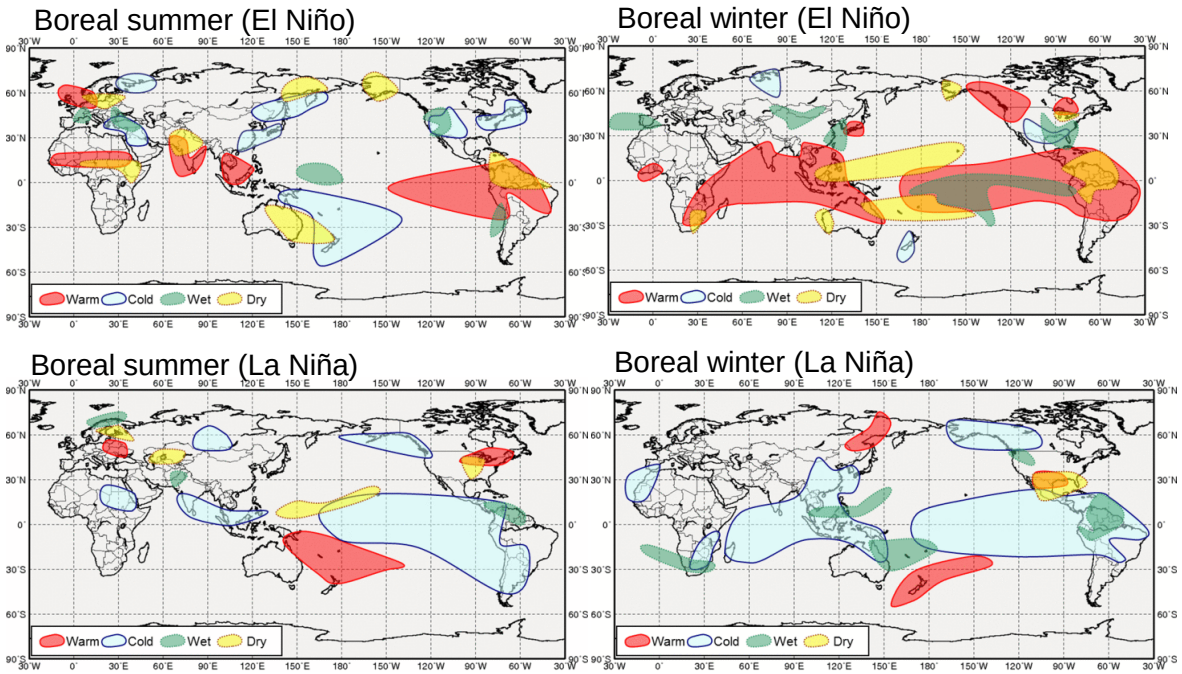


Figure 5 Schematic charts of typical anomaly patterns of surface temperature and precipitation for boreal summer and winter in past El Niño/La Niña events based on the observation and Japanese 55-year Reanalysis (JRA-55) data from 1958 through 2012.

### 3. 2014-16 El Niño event

The Japan Meteorological Agency (JMA) monitors SST in the NIÑO.3 region (5°S–5°N, 150°W–90°W), where interannual variability is the largest in the equatorial Pacific, to identify El Niño/La Niña events. In JMA, El Niño (La Niña) events are defined such that the five-month running mean of NIÑO.3 SST deviation from the latest 30-year average continues +0.5 (-0.5) °C or higher (lower) for six consecutive months or longer. According to this definition, the 2014-16 El Niño event started to develop in boreal summer 2014 (Figure 6). However, five-month running mean of NIÑO.3 SST deviation remained slightly above +0.5 °C of El Niño thresholds until boreal winter 2014/2015 (December 2014 - February 2015). This event strengthened from boreal spring 2015, and the NIÑO.3 SST deviation recorded its peak value of +3.0 °C in December 2015 (Figures 6 and 7). Thereafter, it decayed rapidly and terminated in boreal spring 2016. Duration seasons of this event were 8 seasons (boreal summer 2014 - boreal spring 2016), which is the longest among 15 El Niño events that have occurred since 1949.

The 2014-16 El Niño event was the strongest for 18 years since the El Niño event in 1997-98. During this event, monthly mean NIÑO.3 SST recorded +3.0°C above the latest 30-year average in December 2015. Among fifteen El Niño events that have occurred since 1949, the value of +3.0˚C was third to the two strongest previous El Niño events in 1997-98 and 1982-83 (+3.6 and +3.3 °C, respectively; Figure 8).

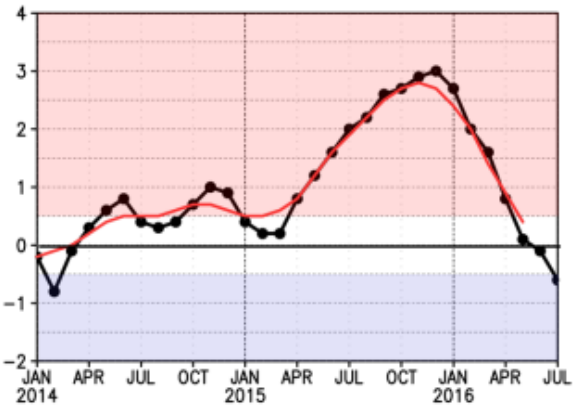


Figure 6 Time series of NINO.3 SST deviation from the latest 30-year average (°C). Black (red) line indicates monthly mean (five-month running mean).

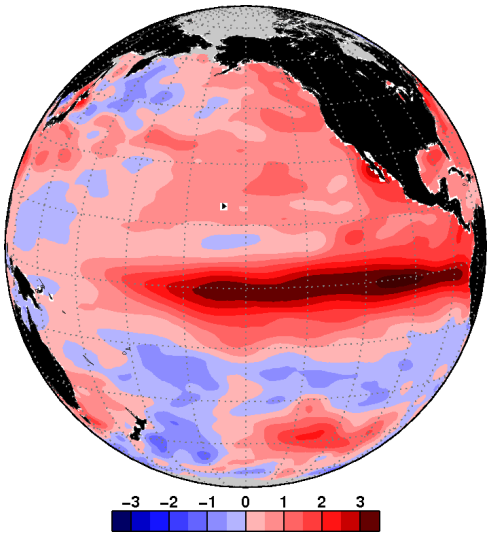


Figure 7 Monthly mean SST in December 2015 (peak of the El Niño event) relative to 1981-2010 mean. Units are °C.

The annual anomaly of the global average surface temperature in 2015 was +0.42°C above the 1981-2010 average, and was the highest since 1891. Global average surface temperature is affected by natural climate variability on interannual to interdecadal time scales in addition to the global warming due to increasing of greenhouse gasses such as $CO_2$. Since the global average surface temperature anomaly varies with a time lag of several months to NINO.3 SST anomaly, the highest temperature record in 2015 could be influenced by the El Niño that began in boreal summer 2014 and developed from boreal spring 2015.

The 2014-16 El Niño event also can be considered to affected to climate in Asia-Pacific region from boreal summer 2015 to boreal winter 2015/2016, high temperatures in low latitudes as well as low precipitations in and around Indonesia. India and Pakistan were suffered from heat waves in May and June 2015, respectively. Six-months-mean temperature from July to

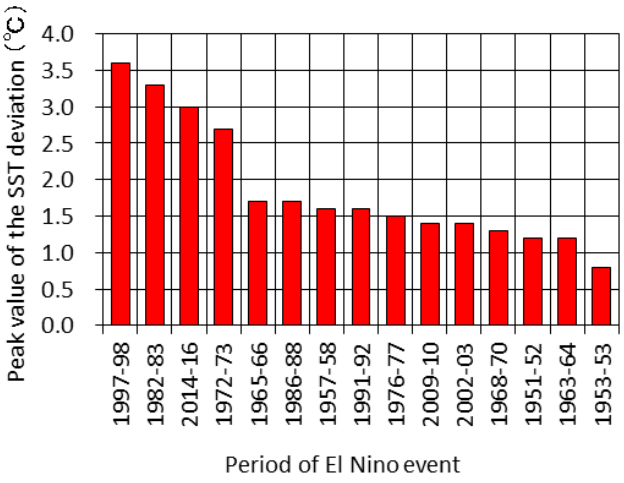


Figure 8 Peak values of NINO.3 SST deviation during each El Niño event since 1949 (°C). The deviation is a departure from the latest 30-year average in each event.

December 2015 for Hyderabad in southern India was 27.4°C that was 2.2°C higher than the normal. The total precipitation amount from September to November 2015 in Banjarmasin in Borneo Island of Indonesia was 113mm that was 19% to the normal. These events were consistent with typical anomaly patterns observed in past El Niño events.

## 4. ENSO diversity

Spatial distribution, amplitude and temporal evolution of ENSO differ from event to event. Figure 9 shows diversity of ENSO that are categorized based on SST anomaly patterns in different ENSO events by Capotondi et al. (2015). The 1997/98 El Niño event shown in right panel has peak of SST anomaly in the eastern part of equatorial Pacific, which is a typical pattern of the canonical El Niño. During 2004-05, on the other hand, the positive SST anomalies peak near the date line, with no significant warming in the eastern part of the equatorial Pacific. The several kind of names for this type of El Niño has been used with different definitions. For example, Ashok et al. (2007) named it "El Niño Modoki" and Kao and Yu (2009) named it "Central Pacific (CP) El Niño". The canonical El Niño events mentioned above are often referred as "eastern Pacific (EP) El Niño". Distribution of ENSO events in longitude–amplitude plane (left panel) shows that both warm and cold events occur over a broad zonal range. It is also noticed that the strongest events occur in the eastern Pacific. EP El Niño events generally have larger amplitudes than EP La Niña events. In the central Pacific, on the other hand, CP La Niña events tend to be slightly stronger than CP El Niño events.

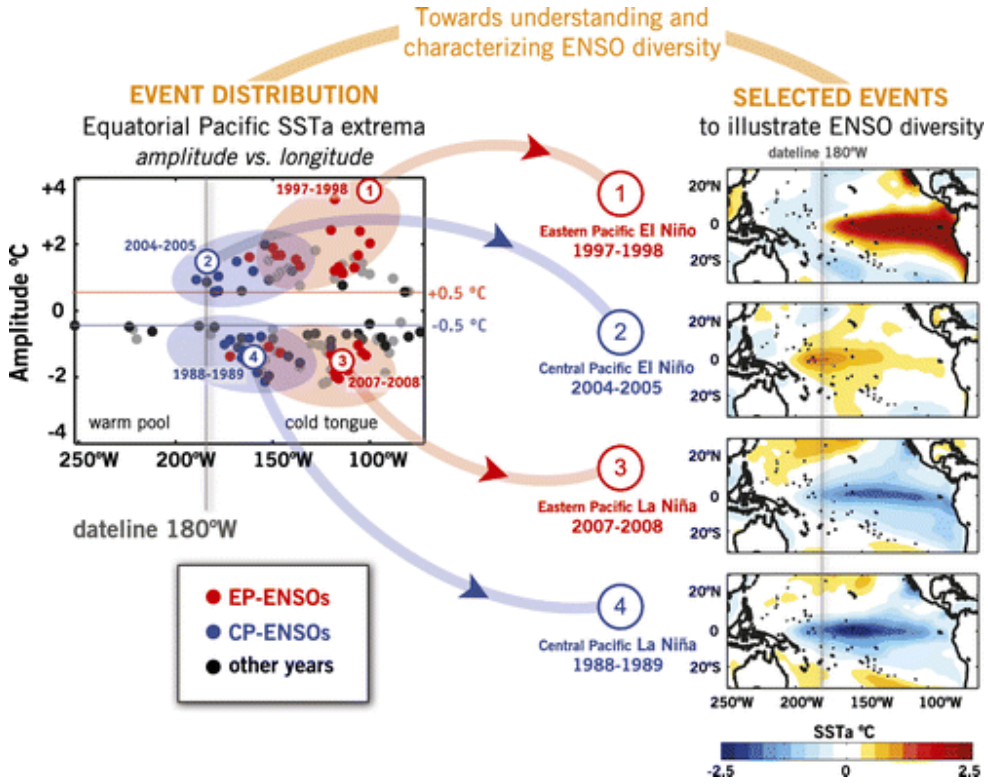


Figure 9 (left) Distribution of boreal winter SST anomaly peaks in the longitude–amplitude plane in the period 1900-2013. Each dot corresponds to the peak value in the region 2°S-2°N, 110°E-90°W. (right) The spatial distributions of SST anomaly for specific warm and cold events of either type. From Capotondi et al. (2015).

## 5. Interannual variability in the tropical Indian Ocean - IOBW and IOD

Recently, it has been widely known that SST variability in the tropical Indian Ocean has a great influence on the climate variability in the Asian and African regions. There are two major SST modes coupled with atmosphere in the tropical Indian Ocean. One is the Indian Ocean Basin Wide (IOBW) mode that the SST anomalies vary uniformly in the tropical Indian Ocean and another is Indian Ocean Dipole (IOD) mode that SST anomalies indicate zonal dipole structure in the tropical Indian Ocean (Saji et al. 1999).

The IOBW has a close correlation with ENSO (Klein et al. 1999). During an El Niño event, SST anomalies in the tropical Indian Ocean increase and the maximum warming of the Indian Ocean occurs from March to May, lagging the peak of SST anomalies in the eastern equatorial Pacific, i.e., El Niño event by about 3 months (left panel of Figure 10). Typically, warmer SST in the Indian Ocean continues until boreal summer, though El Niño event terminates in boreal spring. This positive SST anomalies in boreal summer influence the tropical atmospheric circulation over the northwestern Pacific in addition to the Indian Ocean (Indian Ocean Capacitor Effect: Xie et al. 2009, right panel of Figure 10).

The positive (negative) IOD is typically characterized by negative (positive) SST anomalies in the eastern (western) part of the equatorial Indian Ocean during boreal summer to autumn (Figure 11). The easterlies anomalies and westward shift of active convection area in the equatorial Indian Ocean associated with those SST anomalies further strengthen the zonal gradient of SST anomalies via Bjerknes feedback. Thus, the positive IOD cause a heavy rainfall over the east Africa and droughts over the Indonesian region (Saji et al., 1999; Saji and Yamagata, 2003).

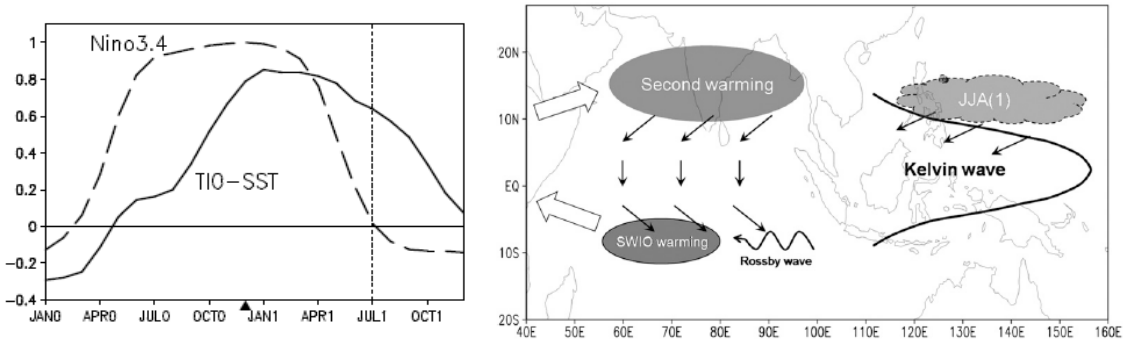


Figure 10 (left) Correlation of tropical Indian Ocean (20°S-20°N, 40°-100°E) SST (solid) with the NINO.3.4 (5°S-5°N, 170°-120°W) SST index for November-January. Numerals in parentheses denote years relative to El Niño: 0 for its developing and 1 for decay year. From Xie et al. (2009). (right) Schematic view of El Niño teleconnection into the Indo-NW Pacific. From Xie et al. (2010).

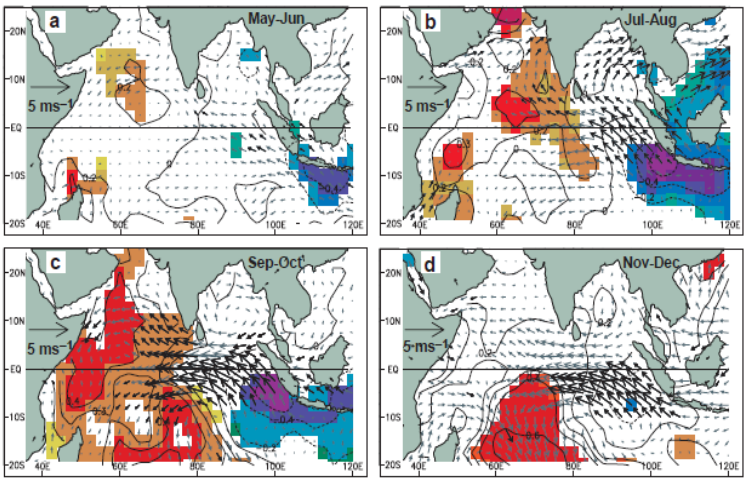


Figure 11 A composite maps of Indian Ocean Dipole (IOD) mode. Evolution of composite SST and surface wind anomalies from May- June, (a) to Nov-Dec (d). Anomalies of SSTs and winds exceeding 90% significance are indicated by shading and bold arrows, respectively. From Saji et al. (1999).

## 6. Pacific Decadal Oscillation (PDO)

The Pacific Decadal Oscillation (PDO, Mantua et al. 1997) is the climate variability in the Pacific with a similar SST pattern but longer time scales (20-30 years) than ENSO (Figure 12). Although PDO is closely related to the decadal variability of ocean biological productivity and the regional climate (Mantua and Hare 2002; Urabe and Maeda 2014), causes for the PDO are not currently known. Recent studies suggested that the slowdown of global warming (global warming hiatus) is associated with a negative phase of PDO that corresponds SST anomaly pattern similar to La Niña events (e.g., Kosaka and Xie 2013).

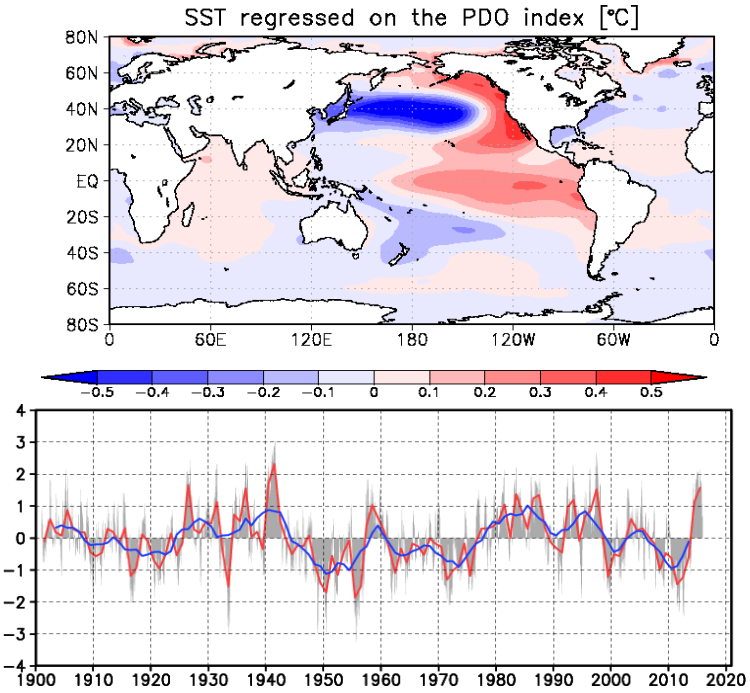


Figure 12 (top) Distribution of monthly SST anomalies linearly regressed on the PDO index. Units are °C. (bottom) Time series of PDO index. Red and blue lines represent annual mean and five-year running mean values, respectively. Gray bars denote monthly values.

## References


Ashok, K., S. K. Behera, S. A. Rao, H. Weng, and T. Yamagata, 2007: El Niño Modoki and its possible teleconnections. *J. Geophys. Res.*, 112, C11007, doi:10.1029/2006JC003798.

Bjerknes, J., 1969: Atmospheric teleconnection from the equatorial Pacific. *Mon. Wea. Rev.*, 97, 163-172.

Capotondi, A. et al., 2015: Understanding ENSO Diversity. *Bull. Amer. Meteor. Soc.*, 96, 921-938, doi: 10.1175/BAMS-D-13-00117.1.

Easterling, D. R., and M. F. Wehner, 2009: Is the climate warming or cooling? *Geophys. Res. Rett.*, 36, L08706.

Jin, F.-F., 1997a: An equatorial ocean recharge paradigm for ENSO. Part I: Conceptual model. *J. Atmos. Sci.*, 54, 811-829.

Jin, F.-F., 1997b: An equatorial ocean recharge paradigm for ENSO. Part II: A stripped-down coupled model. *J. Atmos. Sci.*, 54, 830-847.

Kao, H. Y., and J. Y. Yu, 2009: Contrasting eastern Pacific and central Pacific types of ENSO. *J. Climate*, 22, 615-632, doi:10.1175/2008JCLI2309.1.

Klein, S. A., B. J. Soden, and N. C. Lau, 1999: Remote sea surface temperature variations during ENSO: Evidence for a tropical atmospheric bridge. *J. Climate*, 12, 917-932.

Kosaka, Y., and S. P. Xie, 2013: Recent global-warming hiatus tied to equatorial Pacific surface cooling. *Nature*, 501, 403-407.

Mantua, N. J., S. R. Hare, Y. Zhang, J. M. Wallace, and R. C. Francis, 1997: A Pacific interdecadal climate oscillation with impacts on salmon production. *Bull. Amer. Meteor. Soc.*, 78, 1069-1079.

Mantua, N. J., and S. R. Hare, 2002: The Pacific Decadal Oscillation. *J. Oceanogr.*, 58, 35-44.

Meinen, C. S., and M. J. McPhaden, 2000: Observations of warm water volume changes in the equatorial Pacific and their relationship to El Niño and La Niña, *J. Climate*, 13, 3551-3559.

Philander, S. G. H., 1990: *El Niño, La Niña, and the Southern Oscillation*. Academic Press, 289pp.

Saji, N. H., B. N. Goswami, P. N. Vinayachandran, and T. Yamagata, 1999: A dipole mode in the tropical Indian Ocean. *Nature*, 401, 360-363.

Saji, N. H., and T. Yamagata, 2003: Possible impacts of Indian Ocean Dipole mode events on global climate, *Clim. Res.*, 25, 151-169, 2003.

Schopf, P. S., and M. J. Suarez, 1988: Vacillations in a coupled ocean-atmosphere model. *J. Atmos. Sci.*, 45, 549-567.

Suarez, M. J., and Schopf, P. S., 1988: A delayed action oscillator for ENSO. *J. Atmos. Sci.*, 45, 3283-3287.

Urabe, Y., and S. Maeda, 2014: The relationship between Japan's recent temperature and decadal variability. *SOLA*, 10, 176-179, doi: 10.2151/sola.2014-037.

Xie, S.-P., K. M. Hu, J. Hafner, H. Tokinaga, Y. Du, G. Huang, and T. Sampe, 2009: Indian Ocean capacitor effect on Indo-western Pacific climate during the summer following El Niño, *J. Climate*, 22, 730-747.

Xie, S.-P. Y. Du, G. Huang, X.-T. Zheng, H. Tokinaga, K. Hu, and Q. Liu, 2010: Decadal shift in El Niño influences on Indo-western Pacific and East Asian climate in the 1970s. *J. Climate*, 23, 3352-3368.

Wang, C., and J. Picaut, 2004: *Understanding ENSO physics - A review*, in Earth's Climate: The Ocean-Atmosphere Interaction, Geophysical Monograph Series, Volume 147, edited by C. Wang, S.-P. Xie, and J. A. Carton, pp. 21-48, AGU, Washington, D. C., 2004.

# Primary modes of variability in Earth's climate system

# Primary modes of variability in Earth's climate system

14 November 2016
Yoshinori Oikawa,
Tokyo Climate Center,
Japan Meteorological Agency

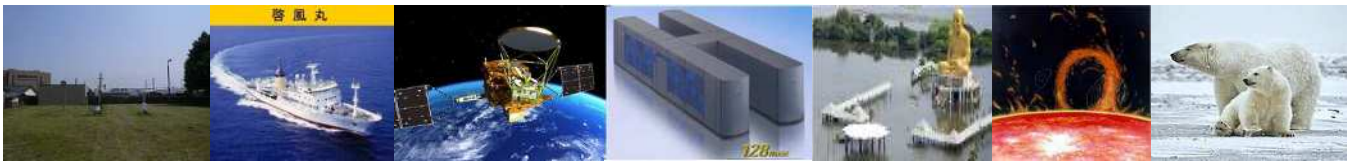


## What is a primary mode of variability?

- On a daily basis, the global atmospheric circulation seems to fluctuate totally at random.
- But a careful statistical analysis reveals a variety of ***preferred circulation patterns*** which emerge on a hemispheric scale.
- Because these preferred patterns tend to develop recurrently and last for weeks or longer, climate researchers recognize them as outstanding. Hence called ***primary modes of variability***.
- By exploiting these preferred patterns, we might have a chance of a better climate analysis and prediction skill.

# Example of a preferred circulation pattern

- In the center figure below, cyclonic and anti-cyclonic anomalies alternate from the equatorial Pacific all the way through North America and reach the Atlantic.
- This represents circulation anomalies known as the (positive) ***Tropical-Northern Hemisphere*** (**TNH**) pattern.
- The negative TNH is defined as a pattern of reversed polarity.
- Positive (negative) TNH is associated with dry (wet) conditions in the southwestern US.

| **Positive** TNH pattern actually seen in Dec. 2013 | **Definition** of TNH pattern (500hPa height anomalies) | **Negative** TNH pattern actually seen in Jan. 2010 |
|---|---|---|

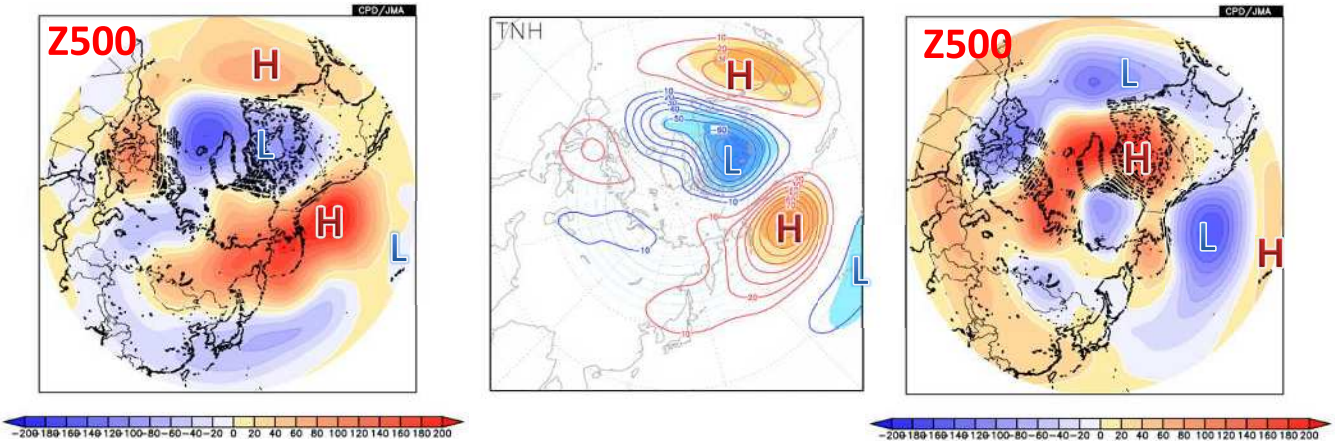


# Teleconnection

- A primary mode of variability is closely related to an important concept of ***Teleconnection***.
- Teleconnection refers to a causal connection of the atmospheric circulation anomalies between remote regions.
- Teleconnection is possible because ***Rossby waves*** (alternate cyclonic and anticyclonic anomalies in the right figure) transport anomalous energy and momentum over a great distance.
- The source of Rossby waves can be often traced back to convection anomalies in the tropics, though this is not always true.

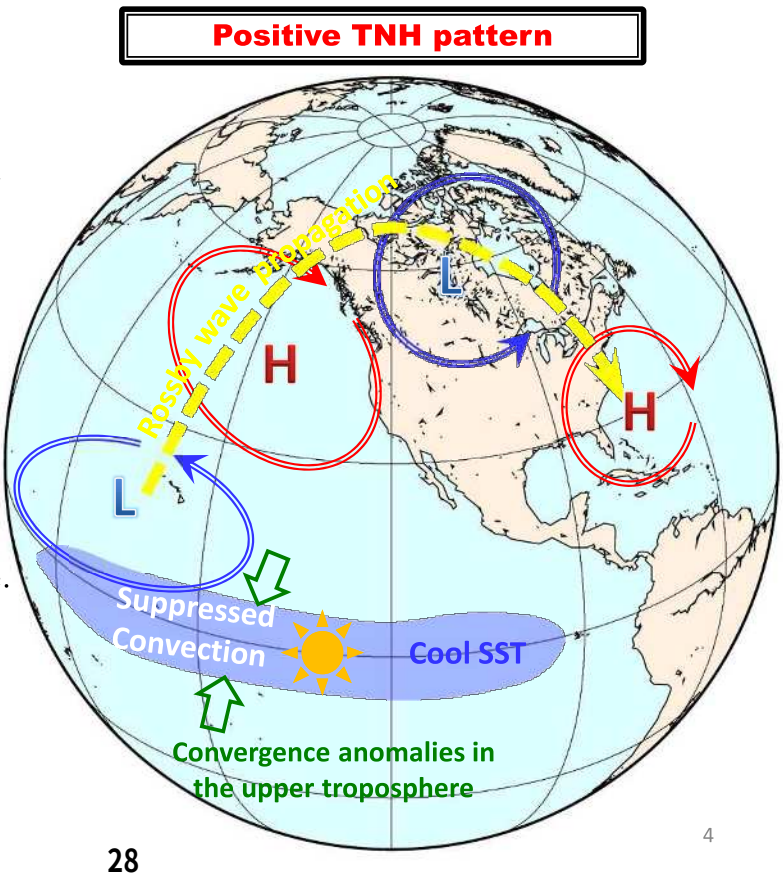

# Primary modes of variability

In the following discussion, we are going to focus our attention on four well-known modes of variability below.

These modes are the most relevant to climate variability in the Asia-Pacific region.

**1) El Niño Southern Oscillation (ENSO)**

**2) Indian Ocean Basin Wide (IOBW)**

**3) Arctic Oscillation (AO)**

**4) Eurasia pattern (EU)**

# El Niño Southern Oscillation (ENSO)

- The most dominant mode of variability in Earth's climate system.
- SSTs in the central to eastern Pacific swing back and forth between a positive (El Niño) and negative (La Niña) phase on a cycle of 2-7 years.
- The influence of ENSO variability on the atmospheric circulation is felt globally through teleconnection.

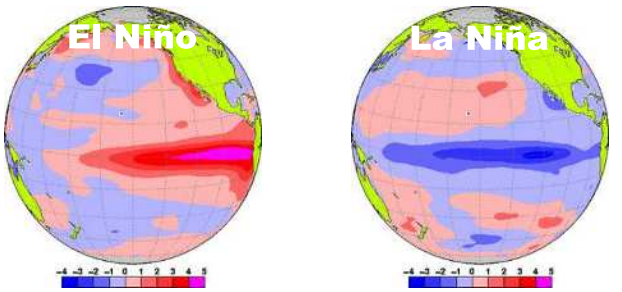


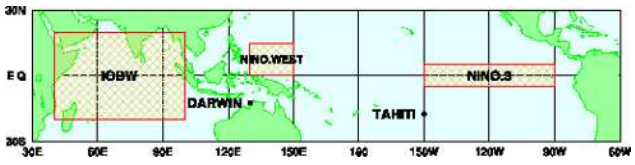


**NINO.3 index**

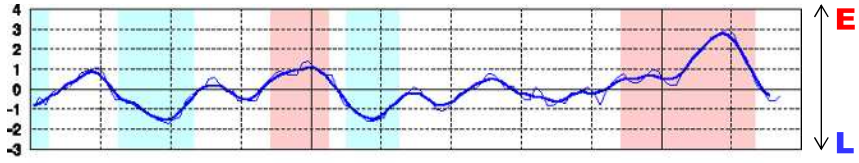


**Southern Oscillation Index**

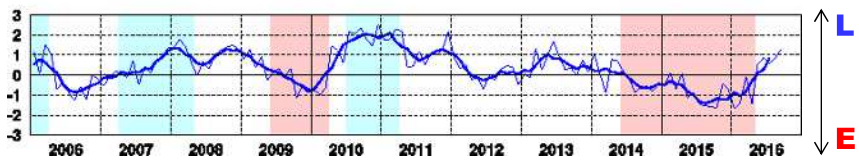


The Southern Oscillation Index is defined as
*SOI = X / SD(X), where X = ANM(Ps(Tahiti))/ SD(Ps(Tahiti)) - ANM(Ps(Darwin))/ SD(Ps(Darwin))*

# Matsuno-Gill pattern

- Gill (1980) elucidated some basic features of the response of the tropical atmosphere to diabatic heating (related to convective activity).

A pair of cyclonic circulation straddling the equator on the western side of the heating (equatorial Rossby wave).

Low pressure and easterly winds along the equator east of the heating (equatorial Kelvin wave).

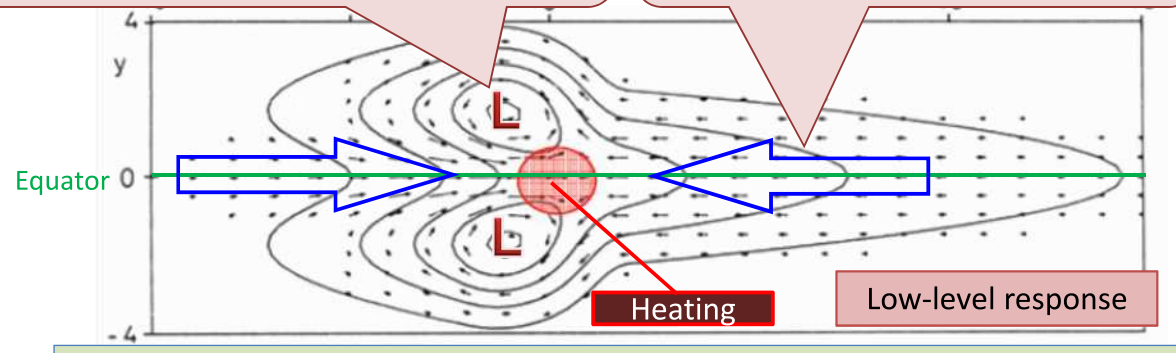


Atmospheric response in the lower troposphere to the heating symmetric about the equator

Contours indicate perturbation pressure, and vectors denote velocity field.
Red circle indicates the position of the heating. (Source: Gill 1980)

Upper-level response shows the reverse of the low-level response.



# El Niño Southern Oscillation

- During an El Niño (La Niña) episode, a significant increase (decrease) in SST over the central to eastern equatorial Pacific is observed.
- The warmer/cooler SSTs lead to convection anomalies in the tropical Pacific.
- These convection anomalies generate Rossby waves, which propagate over a large distance and influence the global atmosphere (teleconnection).

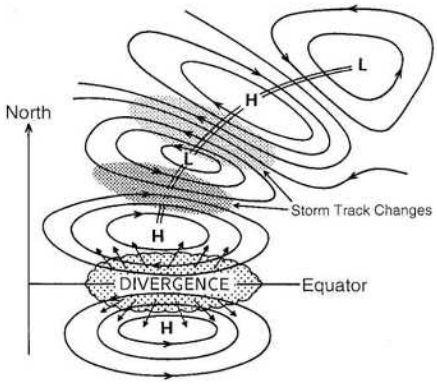


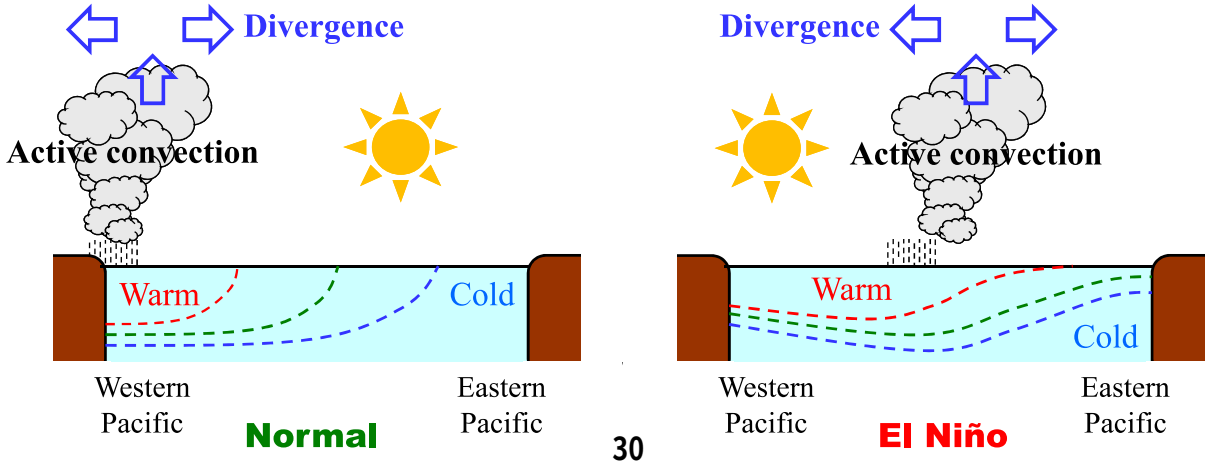

# ENSO and atmospheric circulation (El Niño DJF)

In December to February of El Niño years,

- In the upper troposphere, cyclonic and anti-cyclonic anomalies develop in the western and eastern Pacific, respectively.
- A Rossby wave train extends from cyclonic anomalies centered over South China Sea to the North Pacific.
- In the lower troposphere, anti-cyclonic and cyclonic anomalies develop in the western and eastern Pacific, respectively.

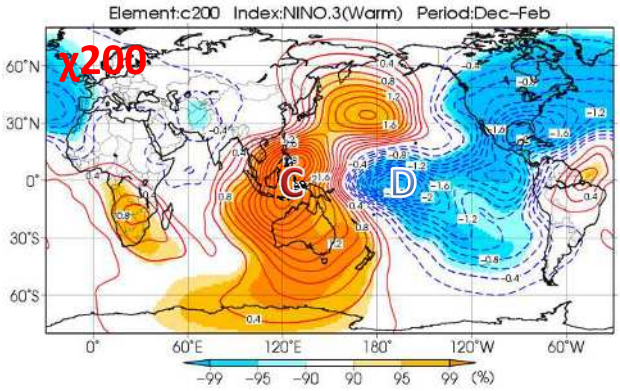


Composite **velocity potential anomalies** for DJF during past El Niño events. "C" and "D" stand for convergence and divergence anomalies, respectively.

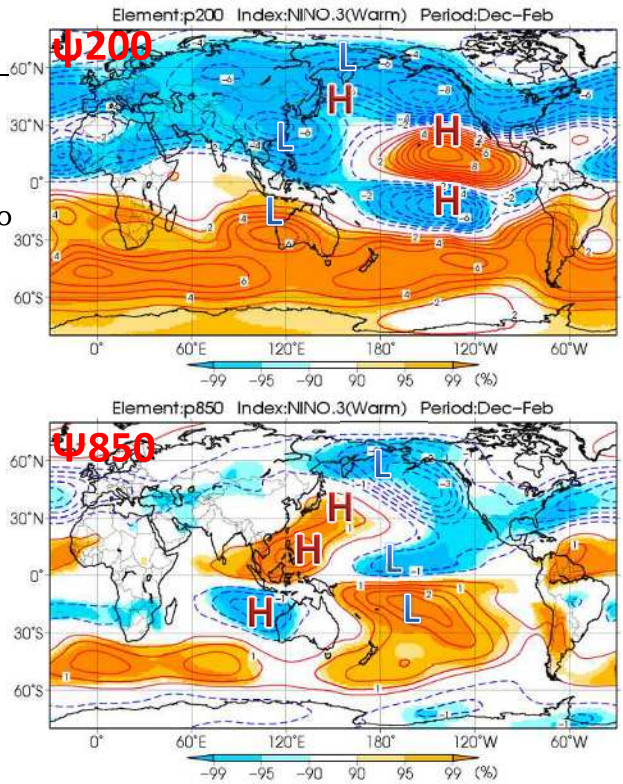


Composite **stream function anomalies** at 200hPa (top panel) and 850hPa (bottom panel) for DJF during past El Niño events


# ENSO and atmospheric circulation (El Niño DJF)

In December to February of El Niño years,

- In the 500hPa height field, positive anomalies extend in the global tropics and to the southeast of Japan, and negative anomalies in the northern North Pacific.
- In the SLP field, positive anomalies extend from the eastern Indian Ocean to the western Pacific and negative anomalies in the eastern Pacific.


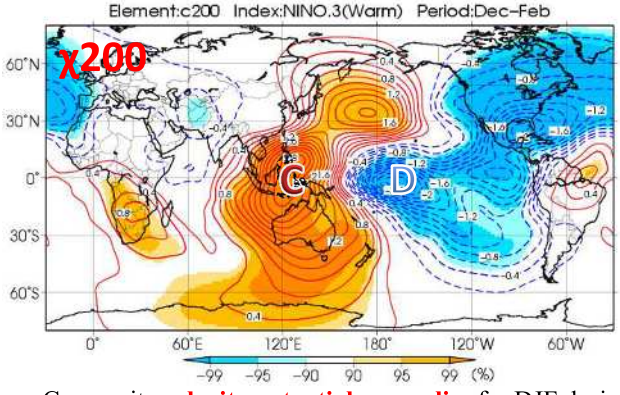


Composite **velocity potential anomalies** for DJF during past El Niño events. "C" and "D" stand for convergence and divergence anomalies, respectively.

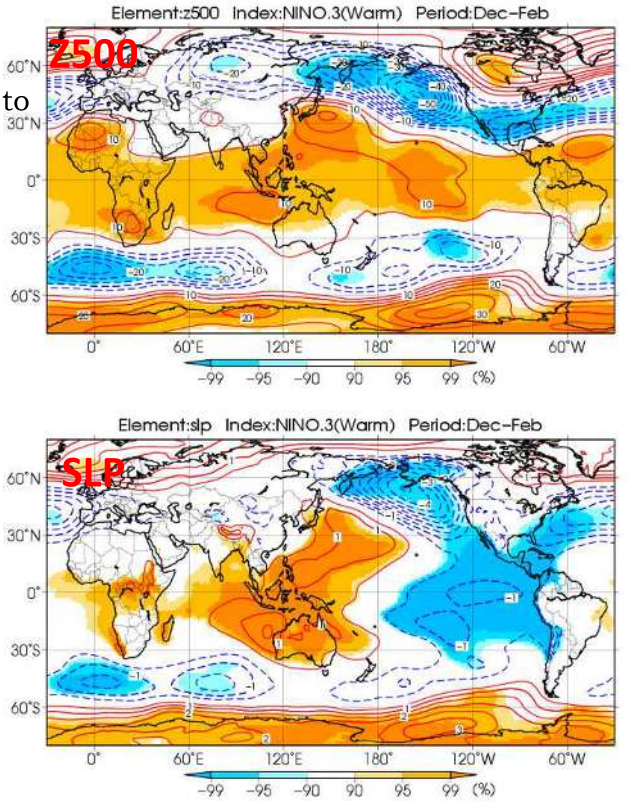


Composite anomalies of **500hPa height** (top) and **SLP** (bottom) for DJF during past El Niño events

# ENSO and atmospheric circulation (La Niña DJF)

In December to February of La Niña years,

- In the upper troposphere, anticyclonic and cyclonic anomalies develop over the Maritime Continent and the eastern Pacific, respectively.
- A Rossby wave train extends from cyclonic anomalies centered over the eastern Pacific to North America, resembling positive TNH.
- In the lower troposphere, cyclonic and anti-cyclonic anomalies develop over the Maritime Continent and the central Pacific, respectively.

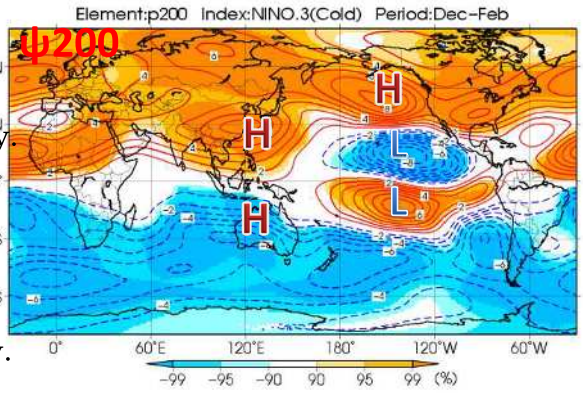


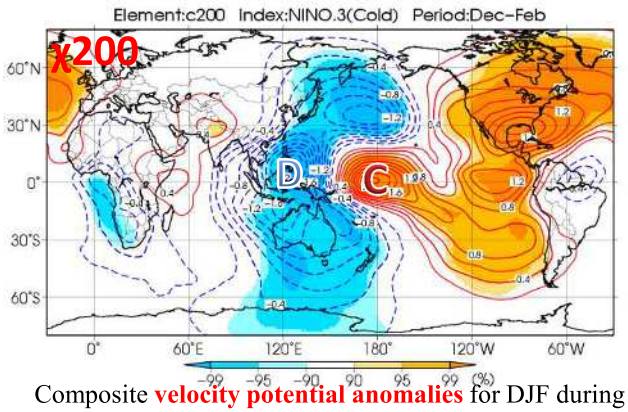


Composite **velocity potential anomalies** for DJF during past La Niña events. "C" and "D" stand for convergence and divergence anomalies, respectively.

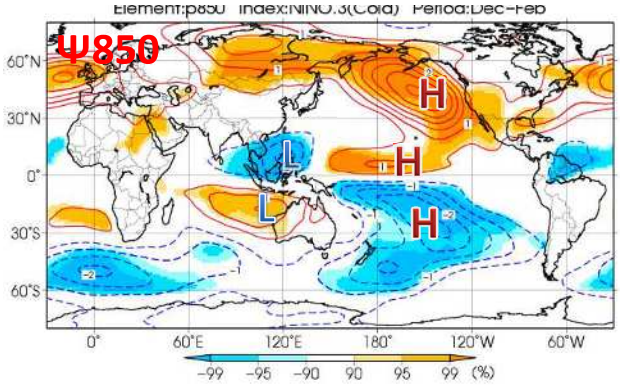


Composite **stream function anomalies** at 200hPa (top panel) and 850hPa (bottom panel) for DJF during past La Niña events

# ENSO and atmospheric circulation (La Niña DJF)

In December to February of La Niña years,

- In the 500hPa height field, negative anomalies extend in the global tropics and positive anomalies in the northeastern North Pacific.
- In the SLP field, positive anomalies extend in the eastern Pacific, and negative anomalies in the Indian Ocean to the western Pacific.

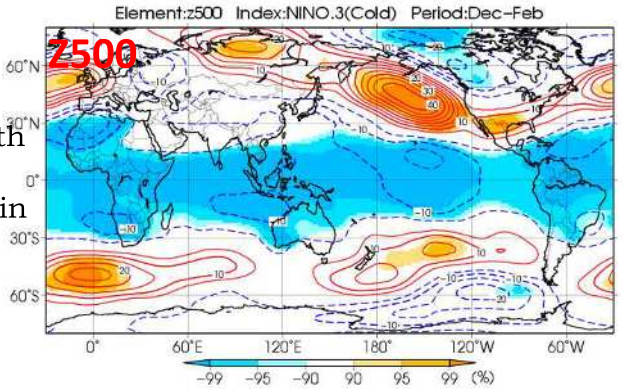


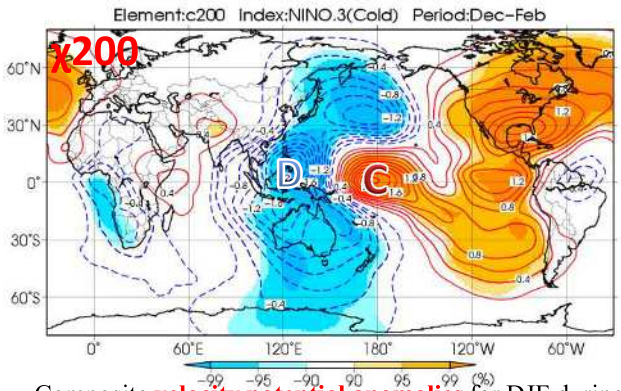


Composite **velocity potential anomalies** for DJF during past La Niña events. "C" and "D" stand for convergence and divergence anomalies, respectively.

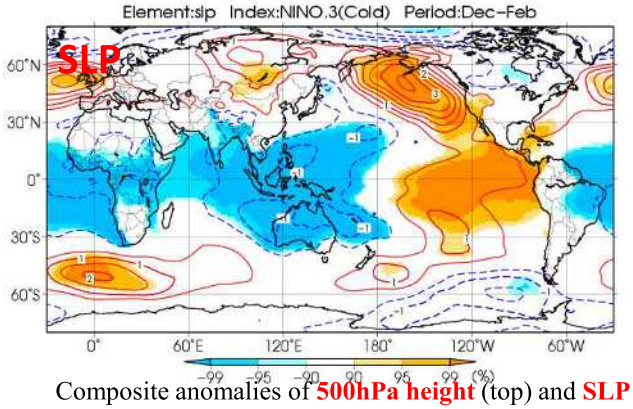


Composite anomalies of **500hPa height** (top) and **SLP** (bottom) for DJF during past La Niña events

# Indian Ocean Basin Wide

- As in the Pacific, SSTs in the Indian Ocean are known to fluctuate between a positive and negative phase basin-wide.
- IOBW tends to follow in the wake of ENSO with a delay of around 3 months.

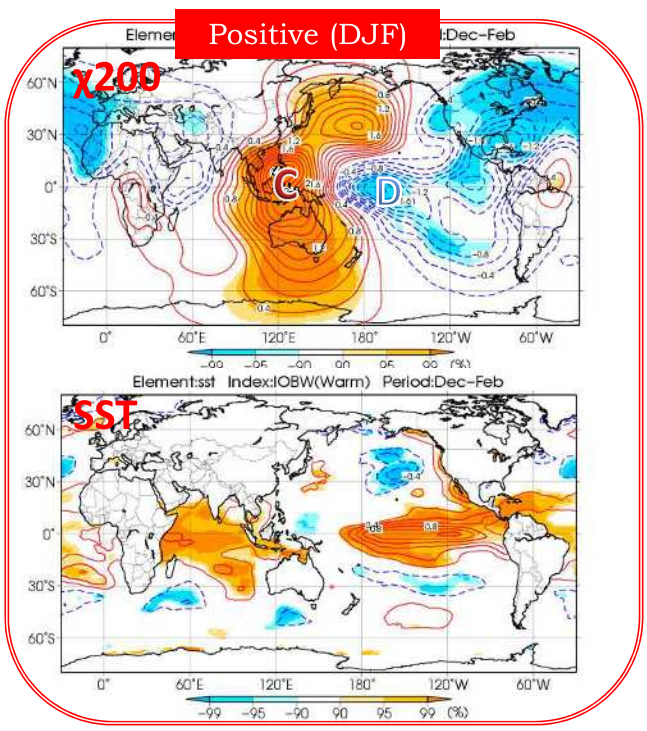


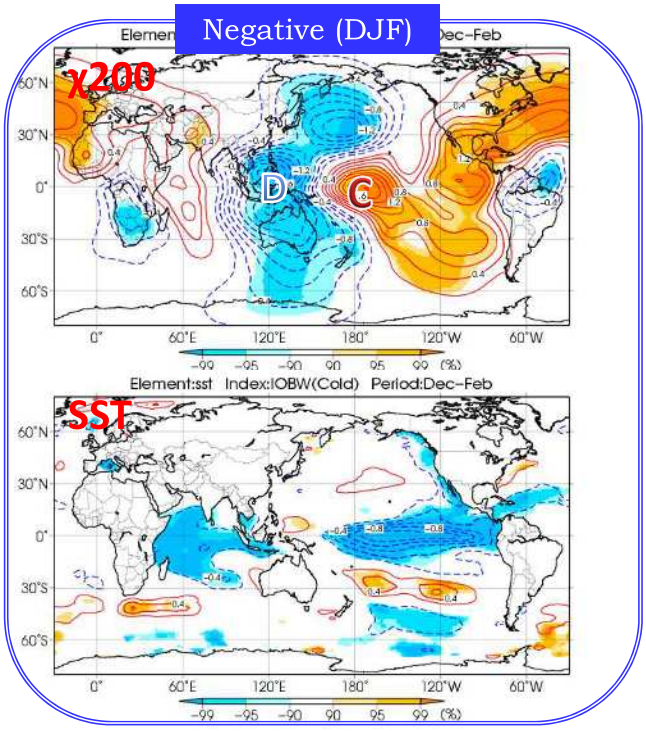


# Indian Ocean Basin Wide

In December to February of positive IOBW years,

- In the upper troposphere, cyclonic and anti-cyclonic anomalies develop in the western and eastern Pacific, respectively. In the lower troposphere, anti-cyclonic and cyclonic anomalies develop over the Maritime Continent and the central Pacific, respectively.

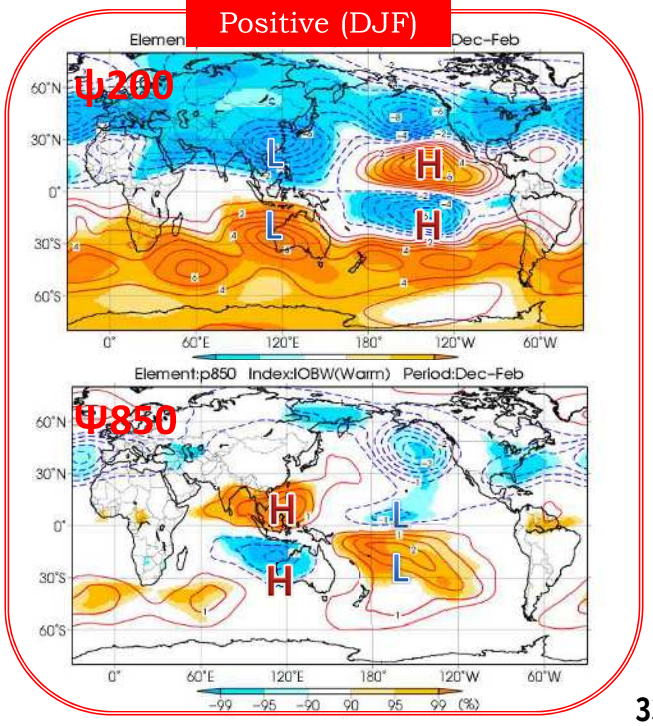


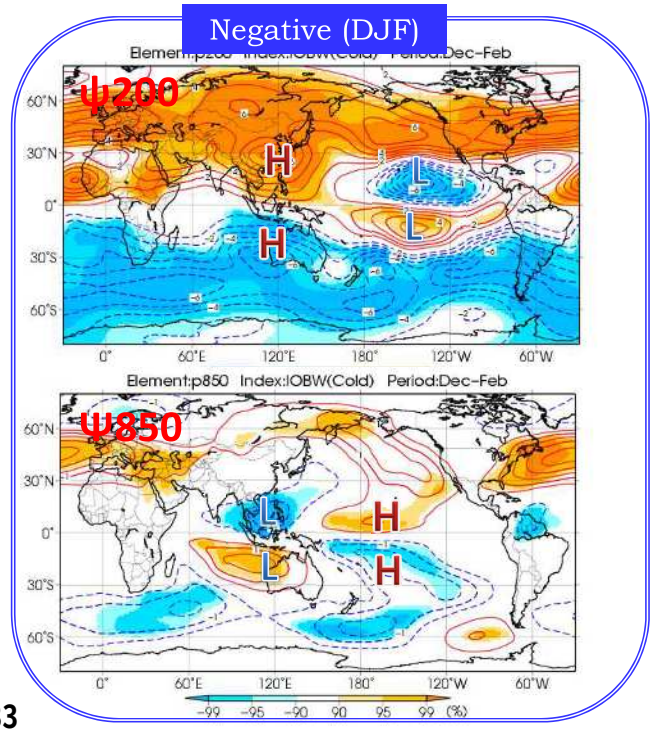

# ENSO/IOBW-related supplementary materials

- For participants' reference, more detailed composite maps of global circulation anomalies associated with ENSO and IOBW are available at the TCC web site. Please visit
  http://ds.data.jma.go.jp/tcc/tcc/products/clisys/enso_statistics/index.html

  or alternatively, it might be much easier to google:

TCC composite map  search

# Arctic Oscillation (AO)

- A seesaw-like oscillation of pressure anomalies between the Arctic and mid-latitudes which dominates climate variability in boreal winter.
- In a positive phase of AO, cold air mass tends to be confined in the Polar region, leading to a warm winter in mid-latitudes.
- In a negative phase of AO, cold air mass flows southward from the Polar region, leading to a cold winter in mid-latitudes.

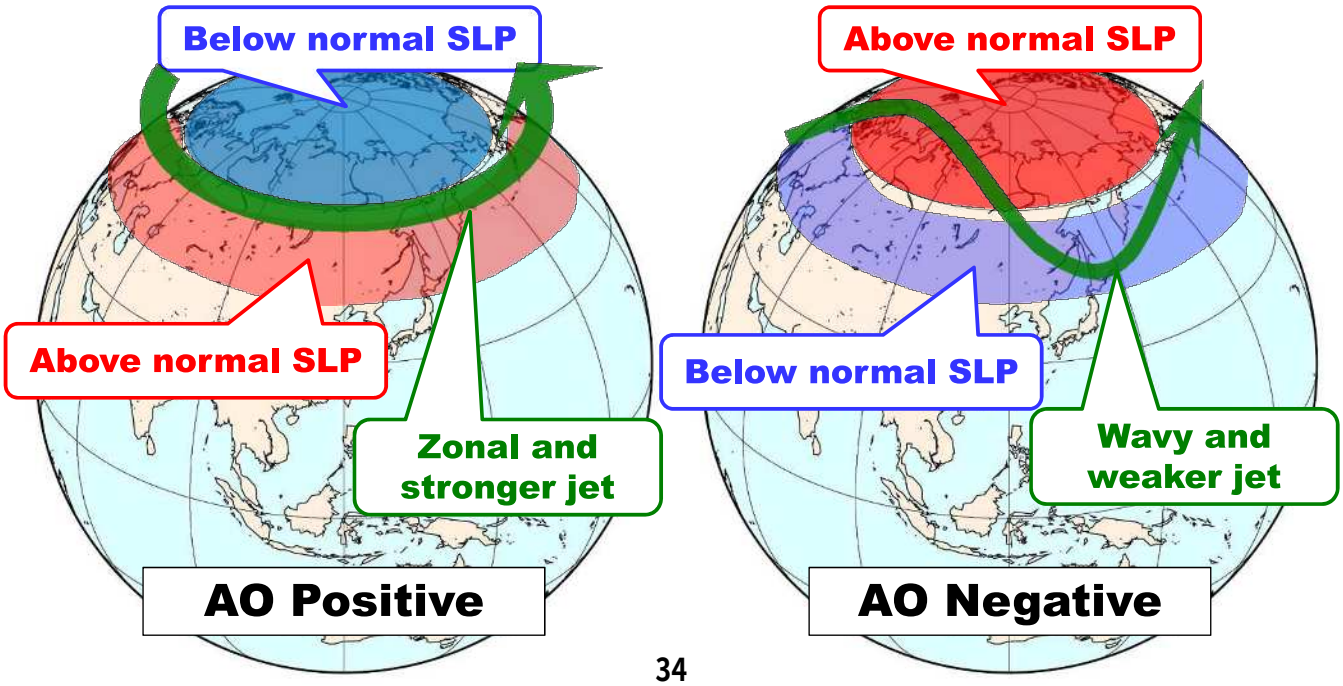

# Definition and AO index

- In the operational analysis at JMA, the AO pattern is defined as the leading mode of Empirical Orthogonal Function (EOF) analysis of monthly mean SLP during 1958-2012 winters (see the central figure below).
- The AO index indicates the degree of similarity between observed SLP anomalies and the defined AO pattern.

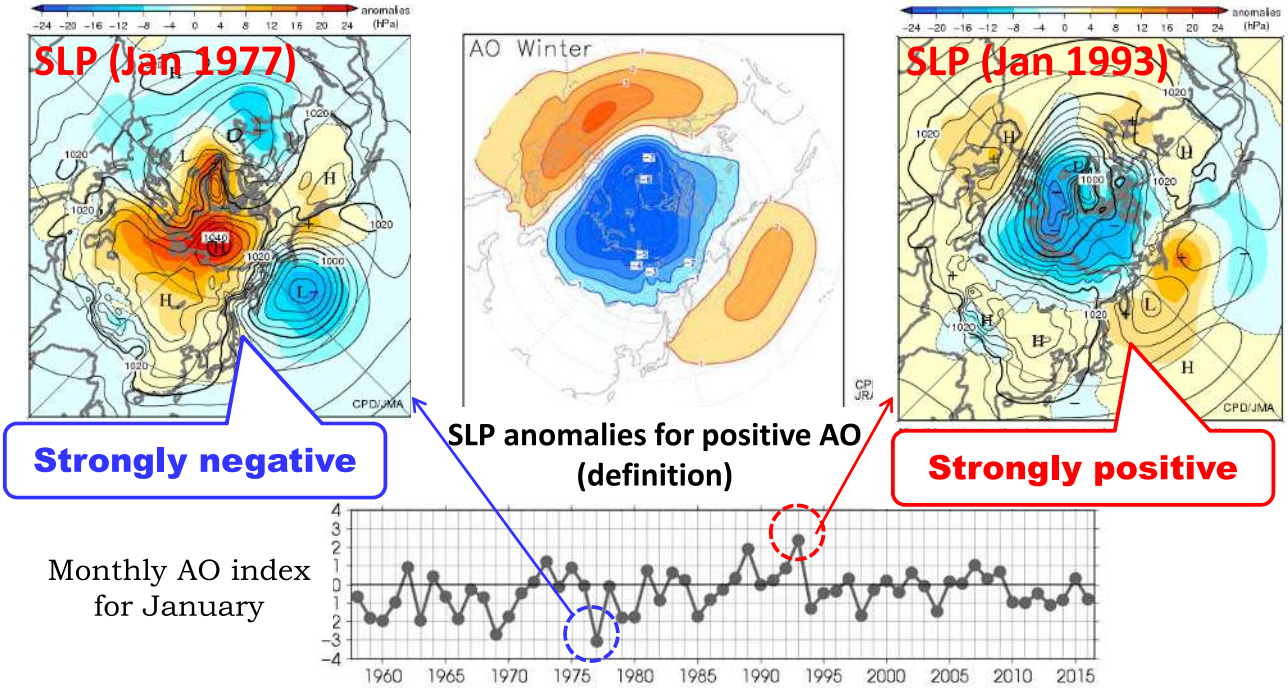


# AO and atmospheric circulation

- Around the end of Dec 2015, the phase of AO suddenly turned from positive to negative.
- In association, Northeast Asia experienced warm December and cold January.

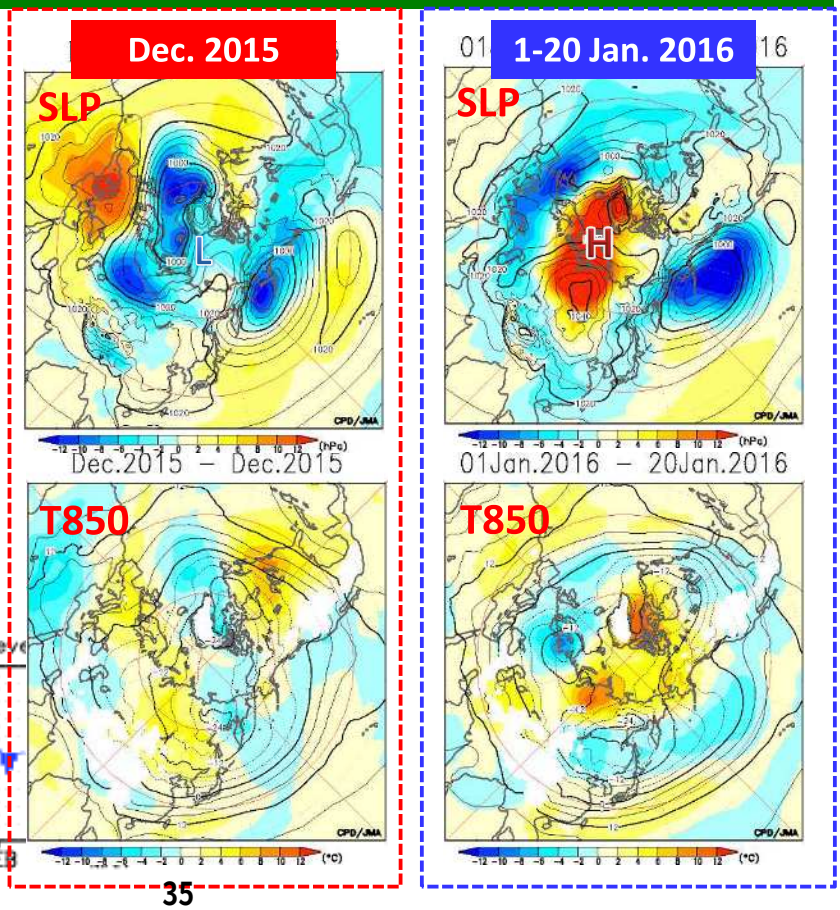


Daily AO index

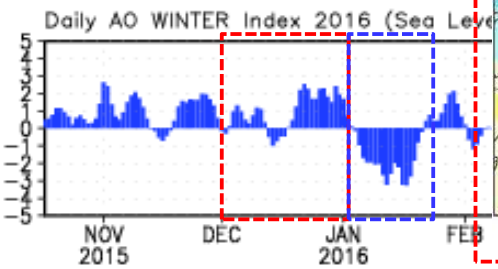

# Eurasia pattern (EU)

- In the operational analysis at JMA, the EU pattern is defined as anomalies in monthly mean 500hPa height field regressed on the EU index during 1958-2012 winters.

- The EU index is composed from monthly mean 500hPa height anomalies at three grid points:

$$EU = -\tfrac{1}{4}z^*(55°N, 20°E) + \tfrac{1}{2}z^*(55°N, 75°E) - \tfrac{1}{4}z^*(40°N, 145°E),$$

- The EU pattern is interpreted as a Rossby wave train extending from the North Atlantic through Siberia down to East Asia along the polar jet stream.

500hPa height anomalies representing the positive EU pattern

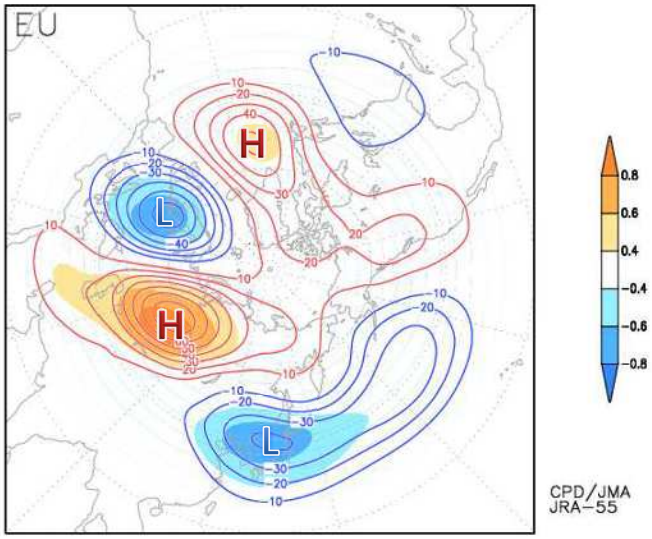


# EU pattern and atmospheric circulation

- The positive EU pattern is associated with an enhanced 500hPa ridge over Siberia (the central figure below) and intensification of the Siberian High (the right figure below).

- Hence the positive EU is often connected to a cold air mass outbreak and leads to an unusually freezing episode over East Asia and sometimes Southeast Asia as well.

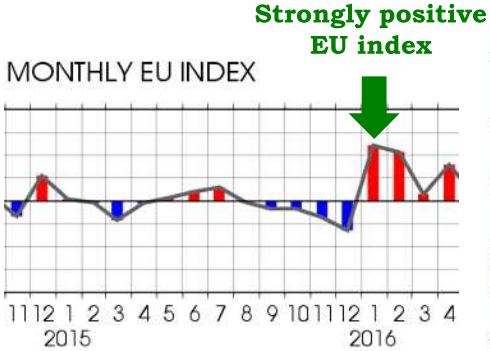


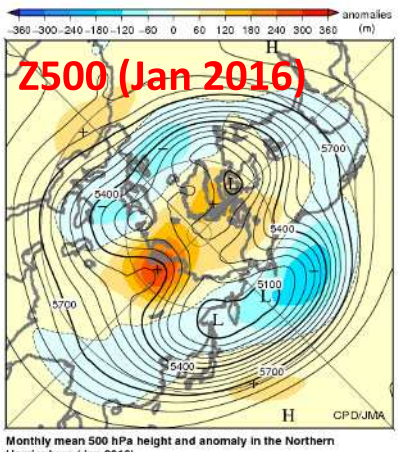


Monthly mean 500 hPa height and anomaly in the Northern Hemisphere (Jan.2016)
The contours show height at intervals of 60 m.
The shading indicates height anomalies.
Anomalies are deviations from the 1981-2010 average.

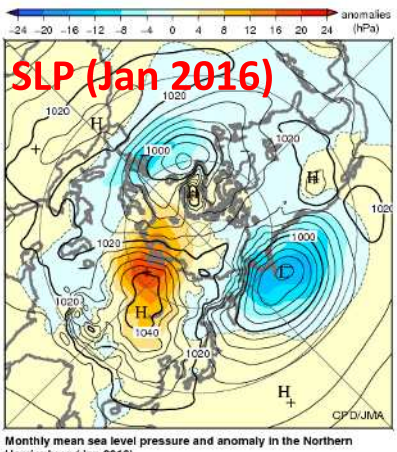


Monthly mean sea level pressure and anomaly in the Northern Hemisphere (Jan.2016)
The contours show sea level pressure at intervals of 4 hPa.
The shading indicates sea level pressure anomalies.
Anomalies are deviations from the 1981-2010 average.

# Other known modes of variability

**P**acific-**N**orth **A**merica pattern

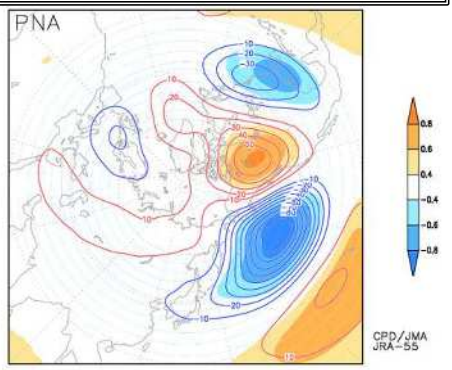


**W**estern **P**acific pattern

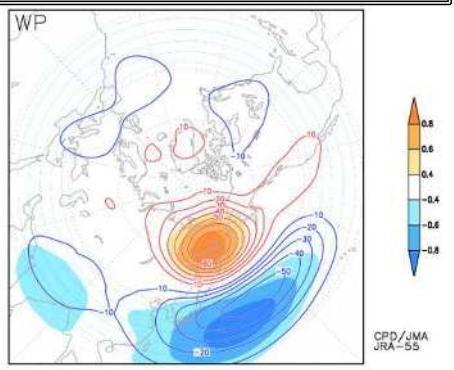


**E**astern **A**tlantic pattern

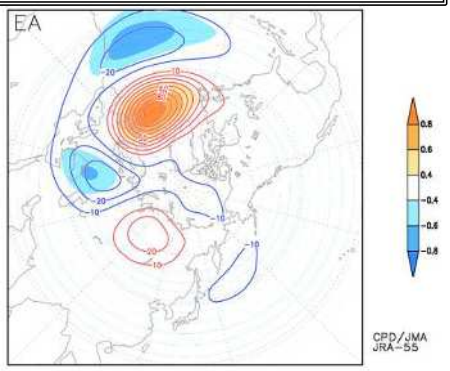


**W**estern **A**tlantic pattern

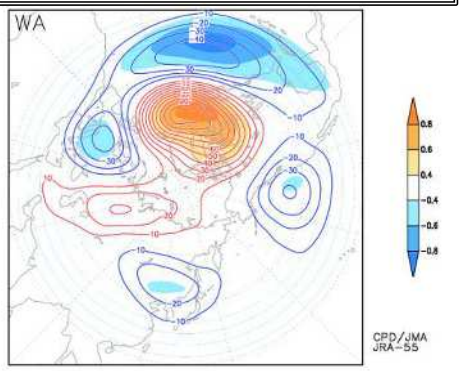


# Some remarks before concluding

- In the exercise session of this seminar, participants are requested to research on a relationship between a primary mode of variability of their choice and climate conditions in their own country.

- So please remind that you are going to discover the mode of variability which is of the greatest concern to your country's climate.

Thank you for your attention.

# Introduction of reanalysis and JRA-55

# Introduction of reanalysis and JRA-55

Masashi HARADA
Climate Prediction Division, Japan Meteorological Agency (JMA)

## 1. Introduction

The main theme of the *TCC Training Seminar 2016* is on *Primary Modes of Global Climate Variability and Regional Climate*. As you will hear in the other lectures, many products for climate monitoring and analysis provided by the TCC/JMA are based on the datasets from Japanese 55-year Reanalysis (JRA-55), the latest reanalysis conducted by the JMA. In this text, outlines of reanalysis and JRA-55 are provided as the basis for climate monitoring and analysis. In addition, two spin-offs of the JRA-55 projects called the JRA-55 sub-product assimilating Conventional observations only (JRA-55C) and the JRA-55 AMIP-type simulation (JRA-55AMIP) are also introduced. In the lecture, the next reanalysis project named the Japanese Reanalysis for Three Quarters of a Century (JRA-3Q), which are currently in preparation, will be explained briefly (though, it is not included in this text).

This document is organized as follows: Background and basis of the reanalysis are outlined in Section 2. Outline of the JRA-55 project, including the data assimilation system and the forecast model as well as basic quality of JRA-55 are provided in Section 3. Section 4 explains the JRA-55 website including the JRA-55 Atlas. Section 5 introduces JRA-55C and JRA-55AMIP.

## 2. Background and basis of reanalysis

### 2.1 Background

Important quantities for climate monitoring and analysis are climatology (long-term mean) and anomaly (deviation from the climatology). In JMA's operational climate monitoring, 1981-2010 average of meteorological variables are used as the climatology, and long-term trends and variations of the anomaly are usually monitored. As the basis for these operations, the climate dataset must be (a) covering the globe for several decades, (b) including as many variables as possible. Furthermore, the dataset needs to be (c) spatially and temporally consistent and highly qualified because the biases in temporal and/or spatial spaces make it difficult to distinguish natural trends and variations of the climate system from artificial ones.

### 2.2 Approaches for producing climate dataset

One approach for producing such a climate dataset is a direct use of observational data. Currently, historical in situ surface and upper air observational data have been accumulated for several decades or a century in many organizations, which could be a reliable data source to

investigate the past climate. Indeed, based on historical observations, a variety of land surface temperature and sea surface temperature (SST) datasets have been developed and used for the climate monitoring. However, conditions (a) and (b) in Section 2.1 are not satisfied in most cases for observational dataset, i.e., (1) observational dataset has a coverage limitation (not distributed uniformly over the globe) and (2) the observed meteorological variables are limited. Consequently, observational dataset alone is generally not sufficient for comprehensive monitoring and analysis of climate.

The other approach is based on a method used in operational numerical weather prediction (NWP). Let us now assume that atmospheric condition at a certain time is estimated by the NWP model with some errors, and observational data before and after the time are given (Fig. 1). For convenience, we further suppose that the observational data are located on grid points of the NWP model. Although it is impossible to know the actual state of the atmosphere, statistical estimation of the atmospheric state by the data assimilation method is possible if we had information on error characteristics of the NWP model and observations. By using the estimated state (hereafter, the analysis) as the initial field for the NWP model, future state can be predicted, which in turn be used as a priori state (hereafter, the first guess) of the next assimilation step.

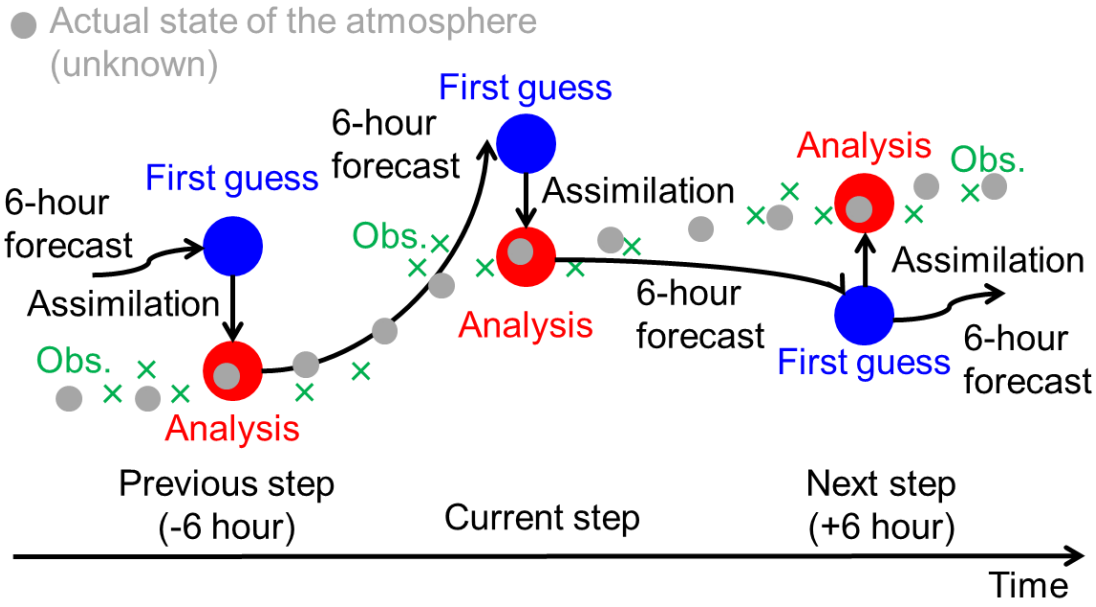


**Fig 1.** Schematic diagram of the analysis cycle. See text for details.

These processes, so-called the analysis cycle, are a continuous repetition of data assimilation and short-term forecasts which aim to estimate the state of the atmosphere as accurate as possible. The accumulated operational analysis dataset contains periodic, three-dimensional, high-quality, and global grid point values (GPV) of many kinds of meteorological variables. Thus, the dataset seems to satisfy the conditions (a), (b) and (c) described above and gives us

the most reliable data for meteorology and climate at the target time. In particular, for climate monitoring, daily global dataset containing many kinds of meteorological variables for several decades are necessary as the basic data.

However, the operational analysis system has two problems from the viewpoint of climate monitoring. The first problem is changes of the NWP model characteristics due to its updates. In the operational NWP centers including JMA, the NWP models are frequently modified to improve its short-term forecast skills. Since the quality of analysis largely depends on performance of the model, changes in the NWP system are problematic for climate monitoring. Thus, the analysis produced with the latest operational system can have a quite different quality from that produced with the older systems. The second problem is a compromised accuracy due to a limited availability of observational data at the time of the operational analysis. Because of time constraints in the near real-time NWP operation, operational systems in general make compromises to cut off belated observational data, which would be available after the cut-off. It is possible that inclusion of these observational data in a delayed analysis could improve the accuracy compared with the operational analysis.

## 2.3 The reanalysis

In order to overcome the problems pointed out in section 2.2, the analysis to produce climate dataset apart from the operational NWP analysis has been conducted at some of the major NWP centers such as the European Center for Medium-Range Weather Forecasts (ECMWF), the National Center for Environmental Prediction (NCEP) and JMA. Here, we define the reanalysis for climate dataset as *"analysis of the past atmospheric conditions using a constant, state-of-the-art NWP and data assimilation system with the latest observation to produce a high-quality, spatially and temporally consistent climate dataset"*.

It should be noted that the NWP model used in the reanalysis are not always the latest one practically because it takes a long time to construct an analysis system and to conduct preliminary investigations before its calculation. Therefore, the *"state-of-the-art"* in the previous paragraph should be added *"as much as possible"* to reserve the time for preparation. In regard to observational data, not all the available observational data are used at the time of reanalysis, but some data are excluded due to the Quality Control (QC) or requirements from the data assimilation system[1]. Hence, *"the latest observation"* in the previous paragraph should also be added as *"quality-controlled and efficient from the viewpoint of assimilation system"*.

[1] JMA's data assimilation system ignores spatial correlation of observational data (non-diagonal elements of the observation error covariance in the data assimilation theory; Kalnay 2003) for computational reasons. Thus, in regions where observational are spatially dense, some data are excluded before the analysis so that the spatial correlation sufficiently decreases (data thinning process).

# 3. Introduction to JRA-55 reanalysis

## 3.1 Overview

The JMA conducted the second Japanese global atmospheric reanalysis, called JRA-55 (Kobayashi et al. 2015). It covers the period starting in 1958, when regular radiosonde observations began on a global basis. JRA-55 is the first comprehensive reanalysis that has covered the last half-century, and is the first one to apply four-dimensional variational (4D-Var) analysis to this period. The main objectives of JRA-55 were to address issues found in previous reanalyses and to produce a comprehensive atmospheric dataset suitable for researches of long-term trends and variability of climate. This section describes forecast model and data assimilation system used to produce JRA-55, as well as the basic characteristics of the JRA-55 product.

## 3.2 Data assimilation system and forecast model used in JRA-55

JRA-55 has been produced with the TL319 version of JMA's operational data assimilation system as of December 2009. The forecast model is based on the TL319 spectral resolution version of the JMA Global Spectral Model (GSM) as of December 2009 (JMA 2013). Both the data assimilation system and forecast model have been extensively improved since the Japanese 25-year Reanalysis (JRA-25, Onogi et al. 2007) as summarized in Tables 1 and 2.

**Table 1.** Data assimilation systems used for JRA-25 and JRA-55.

| | **JRA-25** | **JRA-55** |
|---|---|---|
| Basic system | JMA's operational system<br>as of March 2004 (JMA 2002) | JMA's operational system<br>as of December 2009 (JMA 2007, 2013b) |
| Horizontal grid system | Gaussian | Reduced Gaussian |
| Horizontal resolution | T106 (~110 km) | TL319 (~55 km) |
| **Atmospheric analysis** | | |
| Vertical levels | Surface and 40 levels up to 0.4 hPa | Surface and 60 levels up to 0.1 hPa (Iwamura and Kitagawa 2008; Nakagawa 2009) |
| Analysis scheme | 3D-Var with the T106 inner resolution | 4D-Var with the T106 inner resolution |
| Background error covariances | Static | Static with the simple inflation factor of 1.8 applied before 1972 |
| Bias correction for satellite radiances | *TOVS*<br>Adaptive scheme using 1D-Var analysis departures (Sakamoto and Christy 2009)<br>*ATOVS*<br>Static (until July 2009) and adaptive (thereafter) schemes using radiosonde and supplemental background fields (Kazumori et al. 2004) | VarBC (Derber and Wu 1998; Dee and Uppala 2009; JMA 2013b) |
| Radiative transfer model for satellite radiances | *TOVS:* RTTOV-6<br>*ATOVS:* RTTOV-7 | RTTOV-9.3 |
| **Surface analysis** | | |
| Screen-level analysis | 2D-OI | 2D-OI with the FGAT approach |
| Land surface analysis | Offline SiB<br>with 6-hourly atmospheric forcing | Offline SiB<br>with 3-hourly atmospheric forcing |
| Snow depth analysis | 2D-OI | 2D-OI |

**Table 2.** Forecast models used for JRA-25 and JRA-55.

| | JRA-25 | JRA-55 |
|---|---|---|
| Base model | JMA GSM as of March 2004 (JMA 2002) | JMA GSM as of December 2009 (JMA 2007, 2013b) |
| Horizontal resolution | T106 (~110 km) | TL319 (~55 km) |
| Vertical levels | Surface and 40 levels up to 0.4 hPa | Surface and 60 levels up to 0.1 hPa (Iwamura and Kitagawa 2008; Nakagawa 2009) |
| **Dynamics** | | |
| Horizontal grid system | Gaussian | Reduced Gaussian |
| Advection scheme | Euralian | Semi-Lagrangian |
| **Radiation** | | |
| Longwave radiation | *Line absorptions*<br>Random band model of Goody (1952)<br>*Water vapor continuum (e-type)*<br>Roberts et al. (1976)<br>*Radiatively active gases*<br>$H_2O$, $O_3$ and<br>$CO_2$ (constant at 375 ppmv) | *Line absorptions*<br>Pre-computed transmittance tables and *k*-distribution (Chou et al. 2001)<br>*Water vapor continuum (e-type and p-type)*<br>Zhong and Haigh (1995) with MK_CKD (Clough et al. 2005)<br>*Radiatively active gases*<br>$H_2O$, $O_3$, $CO_2$, $CH_4$, $N_2O$, CFC-11, CFC-12 and HCFC-22 |
| Shortwave radiation | *Absorptions by $H_2O$, $O_2$, $O_3$ and $CO_2$*<br>Briegleb (1992) | *Absorptions by $H_2O$*<br>Briegleb (1992)<br>*Absorptions by $O_2$, $O_3$ and $CO_2$*<br>Freidenreich and Ramaswamy (1999) |
| Cloud radiation | *Longwave*<br>Maximum-random overlap<br>*Shortwave*<br>Random overlap | *Longwave*<br>Maximum-random overlap with the method of Räisänen (1998)<br>*Shortwave*<br>Random overlap |
| Aerosols | Atmospheric aerosol profiles from WMO (1986) (CONT-I over land and MAR-I over sea) | Atmospheric aerosol profiles from WMO (1986) (CONT-I over land and MAR-I over sea) with optical depths adjusted to 2-dimensional monthly climatology |
| **Cumulus convection** | Prognostic Arakawa-Schubert | Prognostic Arakawa-Schubert with DCAPE |
| **Initialization** | Nonlinear normal mode initialization | Not used |
| **Boundary conditions and forcing fields** | | |
| SST and sea ice | COBE-SST (Ishii et al. 2005) | COBE-SST (Ishii et al. 2005) |
| Ozone | T42L45 version of MRI-CCM1 (Shibata et al. 2005) | *Until 1978*<br>Climatology<br>*From 1979 onward*<br>T42L68 version of MRI-CCM1 (Shibata et al. 2005) |

## 3.3 Observation

Observations used in JRA-55 primarily consist of those used in ERA-40 (Uppala et al. 2005) and those archived by JMA. The ERA-40 observational dataset was supplied to JMA by ECMWF for use in the JRA-25 project (Onogi et al. 2007). Observations for the period starting in 1979 are basically the same ones used in JRA-25. In addition, newly available observational datasets were collected and used whenever possible. A detailed list of data suppliers and the type of data provided by them is shown in Table 3.

**Table 3.** Observational data sources for JRA-55. Observations shown in plain cells were added or reprocessed after JRA-25, whereas those in shaded cells are the same as the ones used in JRA-25. Acronyms in this table are summarized in Appendix B. of Kobayashi et al. (2015).

| Data supplier | Data type and supplier's identifiers | Period | Note |
|---|---|---|---|
| **Conventional data** | | | |
| ECMWF | | Jan 1958-Aug 2002 | Uppala et al. (2005) |
| JMA | | Jan 1961- | |
| | GAME and SCSMEX | Apr 1998-Oct 1998 | |
| NCEP/NCAR | SYNOP and upper-level observation | Jan 1979-Dec 1979 | Kalnay et al. (1996)<br>Kistler et al. (2001) |
| M. Yamanaka | Radiosondes from Indonesia | Jan 1958- | Okamoto et al. (2003) |
| M. Fiorino | TCRs | Jan 1958- | Fiorino (2002) |
| RIHMI | Snow depths from Russia | Jan 1958-Dec 2008 | |
| UCAR | Snow depths from USA | Jan 1958-Aug 2011 | NCDC et al. (1981) |
| Monthly Surface Meteorological Data in China | Snow depths from China | Jan 1971-Dec 2006 | Digitized from printed matters |
| IMH | Snow depths from Mongolia | Jan 1975-Dec 2007 | |
| **Satellite radiances** | | | |
| ECMWF | VTPR | Jan 1973-Feb 1976 | Uppala et al. (2005) |
| | HIRS and SSU | Nov 1978-Dec 2000 | |
| | MSU and AMSU | Nov 1978-May 2003 | |
| NOAA/NCDC | SSM/I | Jun 1987-Dec 2004 | |
| NOAA/CLASS | AMSU and MHS | Aug 1998- | |
| | SSM/I | Jul 1987- | |
| JMA | AMSU and MHS | Jun 2003- | |
| | SSM/I and SSMIS | Mar 2006- | |
| | TMI | Dec 2011- | |
| | CSR | Jun 2005- | |
| JMA/MSC | Reprocessed CSRs from GMS-5, GOES 9 and MTSAT-1R | Jul 1995-Dec 2009 | |
| JAXA, NASA | Reprocessed TMI version 7 | Feb 1998-Dec 2011 | |
| JAXA | Reprocessed AMSR-E Version 3 | Jun 2002-Oct 2011 | |
| EUMETSAT | CSRs from the Meteosat series | Jan 2001-Aug 2009 | |
| **AMVs** | | | |
| ECMWF | GMS, Meteosat and GOES | Jan 1979-Dec 1997 | Uppala et al. (2005) |
| JMA | GMS, MTSAT, Meteosat and GOES | Dec 1979-Dec1980, Jan 1998- | |
| | MODIS | Jun 2004- | |
| JMA/MSC | Reprocessed GMS, GOES 9 and MTSAT-1R | Jan 1979-Nov 1979<br>Nar 1987-Sep 2009 | |
| EUMETSAT | Reprocessed Meteosat-2 | May 1982-Aug 1988 | van de Berg et al. (2002) |
| | Reprocessed Meteosat-3 and -7 | Jan 1989-Dec 2000<br>Aug 1988-Nov 1998 | |
| | Meteosat-5 and -7 | Jan 2001-Feb 2001 | |
| **Scatterometer ocean surface winds** | | | |
| ESA | Reprocessed AMI (ERS.ASPS20.N) | May 1997-Jan2001 | De Chiara et al. (2007) |
| Hersbach (2008) | | | |
| JPL | Reprocessed SeaWinds from QuickSCAT (QSCAT_LEVEL_2B_V2) | Jul 1999-Nov 2009 | Dumbar et al. (2006) |
| JMA | ASCAT | Jan 2008- | |
| **GNSS-RO refractivities** | | | |
| CDAAC | Reprocessed CHAMP, SAC-C, COSMIC, GRACE, Metop-A, TerraSAR-X, and C/NOFS | Jul 2006-Jun 2012 | |
| JMA | COSMIC, GRACE, Metop, TerraSAR-X, and C/NOFS | | |

## 3.4 Basic performance of JRA-55

Kobayashi et al. (2015) investigated performance of JRA-55 to reproduce long-term variation and/or climatological distribution of basic meteorological variables such as temperature, precipitation, and sea-level pressure. Harada et al. (2016) extended their analysis to include stratospheric circulation, global distributions of tropical cyclones, the Madden-Julian oscillation, and mid-latitude storm tracks. These two papers conclude that the JRA-55 products are considerably better than the JRA-25. In this subsection, some examples from these two papers are presented. Some of the other topics not included in this text will be explained in the lecture.

### 3.4.1 Two-day forecast scores

To evaluate the temporal consistency of the product and the impact of changes in observing systems, a short-range forecast was carried out from 12 UTC every day in JRA-55. Fig. 2 shows the time series of RMS errors in 2-day forecasts of a geopotential height at 500hPa averaged over the extratropical northern and southern hemisphere from JRA-25, JRA-55, and the JMA operational system, as verified against their own analyses. Although the comparison is not made based on a common standard, it can provide useful insights regarding the temporal consistency of each product.

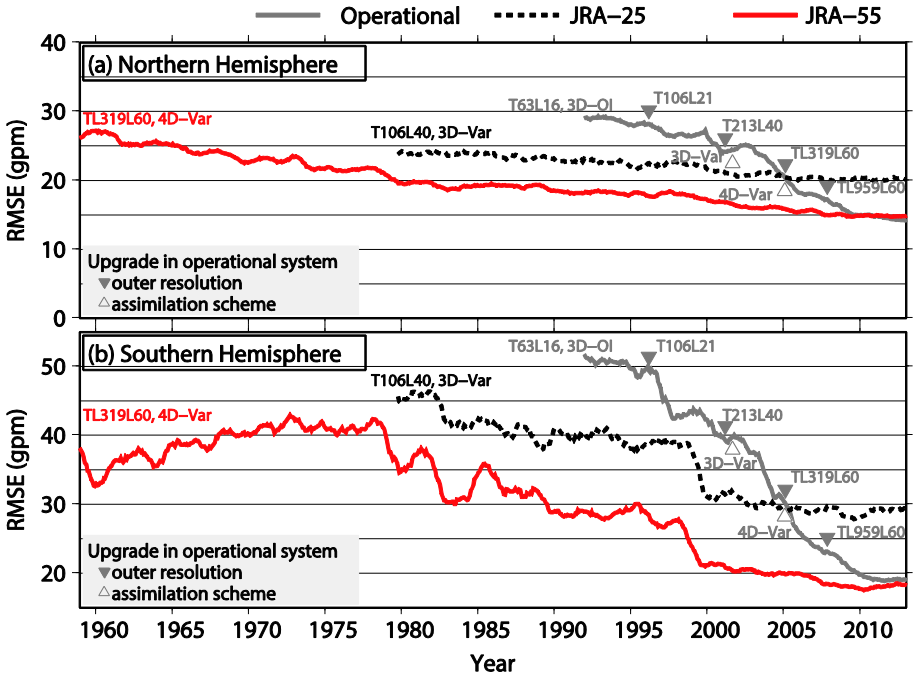


**Fig. 2.** RMS (Root Mean Square) errors of 2-day forecasts of the geopotential height at 500hPa averaged over the extratropics of the (a) Northern and (b) Southern Hemispheres from JRA-25, JRA-55 and JMA operational system, verified against their own analyses. Changes in the assimilation scheme and resolution of the outer model are also noted. Each value represents the average for the last 12 months.

The JMA operational system has been improved in many aspects since JRA-25, including a revision of the longwave radiation scheme and the introduction of 4D-Var and VarBC (section 3.2). The JRA-55 data assimilation system incorporates these improvements and has been used consistently throughout the reanalysis period. Therefore, variations in the forecast scores of JRA-55 can be attributed solely to the changes in observing systems and natural variations of atmospheric predictability, whereas forecast scores of the operational system strongly depend on the effect of these improvements. These are evidence of the greater temporal consistency of the JRA-55 product. The forecast scores of the JRA-55 system are considerably better than those of the JRA-25 system and the improvement of forecast scores is particularly significant in the southern hemisphere, which is most likely because of the availability of new satellite observations as well as the improvement of the data assimilation system.

### 3.4.2 Temperature

Fig. 3 compares monthly mean land-surface air temperature anomalies from the Climatic Research Unit (CRU) temperature database (CRUTEM4, Jones et al. 2012), the NCEP/National Center for Atmospheric Research (NCAR) reanalysis, ERA-40, JRA-25, and JRA-55, averaged over the globe. Reanalyses are sampled with the same spatial and temporal coverage as CRUTEM4. The screen-level analysis method used for JRA-55 is basically the same as the one used for JRA-25, and the low-frequency variability of 2-m temperature anomalies over land is fairly similar in the two reanalyses. Compared with ERA-40, the trend reproduced in JRA-55 is closer to that in CRUTEM4 but there is a difference of less than 0.1 K in warming between CRUTEM4 and JRA-55 after the 1990s. The difference might be related to a difference in method to use observations between CRUTEM4 and JRA-55. In JRA-55, observations on islands and the coast are not used in the screen-level analysis of JRA-55 and analysis in those areas could be affected by observations in coastal waters such as reports of surface observation from sea stations (SHIP) and buoy observations (BUOY), and by SST through background fields. On the other hand, CRUTEM4 is based on observations over land only, which include those on islands and on the coast.

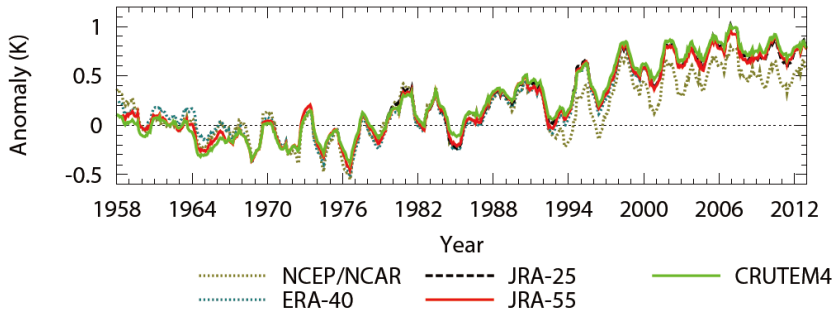


**Fig. 3.** Twelve-month running mean land-surface air temperature anomalies from CRUTEM4, the NCEP/NCAR reanalysis, ERA-40, JRA-25, and JRA-55, averaged over

the globe. Anomalies for each dataset were defined relative to their own climatological monthly means over 1961–1990, except JRA-25, for which anomalies were first computed relative to its own climatological monthly means over 1981–2010 and then adjusted so that their average over 1979–1990 gave the same value as that of JRA-55. Reanalyses are sampled with the same spatial and temporal coverage as CRUTEM4.

### 3.4.3 Precipitation

Fig. 4 shows the climatological distribution of precipitation in JRA-55, JRA-25, ERA-Interim (Dee et al. 2011), ERA-40, the Modern-Era Retrospective Analysis for Research and Applications (MERRA, Rienecker et al. 2011), and the Global Precipitation Climatology Project (GPCP) version 2.2 (Adler et al. 2003) as an observational dataset. While precipitation in middle and high latitudes are underestimated in most reanalyses, JRA-55 well reproduce these feature, especially in the Pacific and Atlantic Oceans north of 30°N. On the other hand, JRA-55 overestimates precipitation in the tropics compared with GPCP. The regions where JRA-55 overestimates precipitation tend to exhibit the spin-down problem (precipitation is excessive immediately after the start of forecasts and then gradually decreases) (not shown). Therefore, the excessive precipitation in the tropics in JRA-55 is most likely related to the dry bias and the spin-down problem of the forecast model in regions of deep convection.

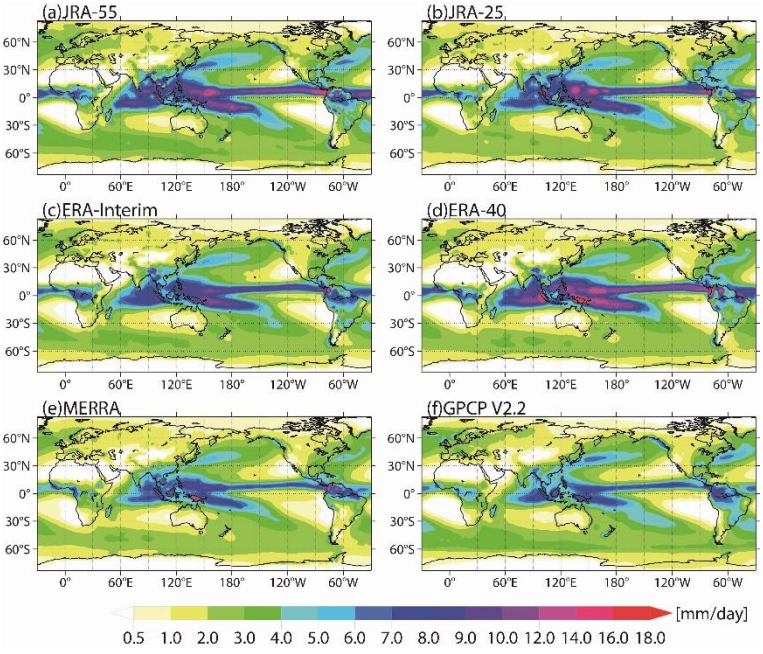


**Fig. 4.** Climatological annual mean precipitations in (a) JRA-55, (b) JRA-25, (c) ERA-Interim, (d) ERA-40, (e) MERRA, and (f) GPCP V2.2, averaged over 1980–2001.

## 4. JRA-55 homepage and Atlas

The JRA-55 data are available from the JMA Data Distribution System (JDDS) for registered users. Registration application can be made at the JRA-55 homepage by filling in necessary information such as purpose of use. The dataset is also available from the Data Integration and

Analysis System (DIAS) managed by the University of Tokyo, the Center for Computational Sciences (CCS) of University of Tsukuba, NCAR in the US, and the Earth System Grid Federation (ESGF) at the National Aeronautics and Space Administration (NASA). Note that registration at the JRA-55 homepage is valid only at JDDS. Separate registration is required for downloading from these collaborative organizations.

The JRA-55 homepage also contains the JRA-55 Atlas, which provides climate maps for a variety of meteorological variables ranging from basic metrics such as surface temperature and wind to technical considerations for climate research (Fig. 5). It is expected to be widely useful in research and education.

JRA-55 homepage: http://jra.kishou.go.jp/JRA-55/index_en.html
JRA-55 Atlas: http://ds.data.jma.go.jp/gmd/jra/atlas/en/index.html

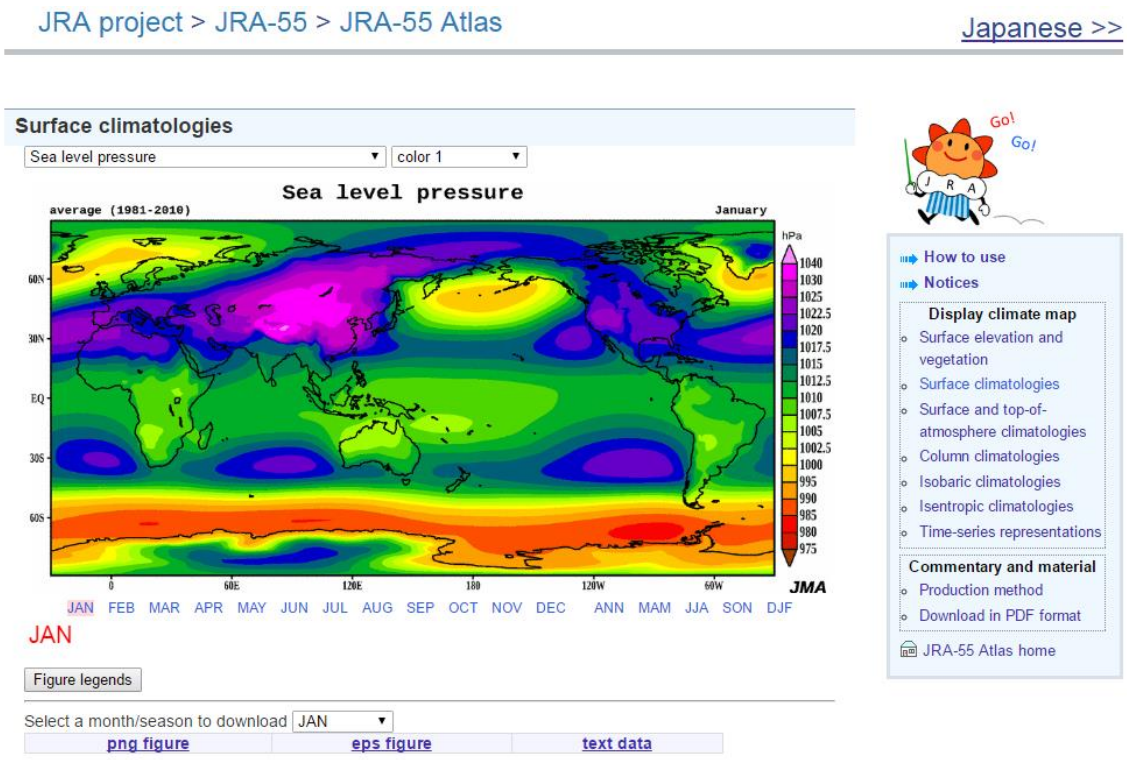


**Fig. 5.** Climatology of sea level pressure shown in the JRA-55 Atlas

## 5. JRA-55C and JRA-55AMIP

As spin-offs of the JRA-55 project, the Meteorological Research Institute (MRI) of JMA has produced two sub-products. The first one, named JRA-55C (Kobayashi et al. 2014), assimilates only conventional surface and upper air observations, with no use of satellite observations, using the same data assimilation system as used for JRA-55. This sub-product aims to produce a more homogeneous dataset over a long period, unaffected by changes in historical satellite

observing systems. The dataset is intended to be suitable for researches of climate change or multi-decadal variability. The other one, named JRA-55AMIP, has been carried out by prescribing the same boundary conditions and radiative forcing of JRA-55, such as the historical observed sea surface temperature, sea ice concentration, greenhouse gases, with no use of atmospheric observational data. This sub-project is intended to assess systematic errors of the model. These datasets are available from the DIAS and NCAR websites.

## References


Adler, R. F., G. J. Huffman, A. Chang, R. Ferraro, P.-P. Xie, J. Janowiak, B. Rudolf, U. Schneider, S. Curtis, D. Bolvin, A. Gruber, J. Susskind, P. Arkin, and E. Nelkin, 2003: The Version-2 Global Precipitation Climatology Project (GPCP) monthly precipitation analysis (1979-present). J. Hydrometeor., 4, 1147-1167.

Briegleb, B. P., 1992: Delta-Eddington approximation for solar radiation in the NCAR community climate model. J. Geophys. Res., 97, 7603–7612.

Chou, M.-D., M. J. Suarez, X.-Z. Liang, and M. M.-H. Yan, 2001: A thermal infrared radiation parameterization for atmospheric studies. Technical report series on global modeling and data assimilation, NASA/TM-2001-104606, 19, National Aeronautics and Space Administration (NASA) Goddard Space Flight Center, USA, 68 pp.

Clough, S. A., M. W. Shephard, E. J. Mlawer, J. S. Delamere, M. J. Iacono, K. Cady-Pereira, S. Boukabara, and P. D. Brown, 2005: Atmospheric radiative transfer modeling: a summary of the AER codes. J. Quant. Spectrosc. Radiat. Transfer, 91, 233–244.

De Chiara, G., R. Crapolicchio, and P. Lecomte, 2007: ERS-1/2 scatterometer new products: mission reprocessing and data quality improvement. Paper presented at the 2nd Space for Hydrology Workshop, Geneva, Switzerland, November, 12-14, 2007.

Dee, D. P., S. M. Uppala, A. J. Simmons, P. Berrisford, P. Poli, S. Kobayashi, U. Andrae, M. A. Balmaseda, G. Balsamo, P. Bauer, P. Bechtold, A. C. M. Beljaars, L. van de Berg, J. Bidlot, N. Bormann, C. Delsol, R. Dragani, M. Fuentes, A. J. Geer, L. Haimberger, S. B. Healy, H. Hersbach, E. V. Hólm, L. Isaksen, P. Kållberg, M. Köhler, M. Matricardi, A. P. McNally, B. M. Monge-Sanz, J.-J. Morcrette, B.-K. Park, C. Peubey, P. de Rosnay, C. Tavolato, J.-N. Thépaut, and F. Vitart, 2011: The ERA-Interim reanalysis: configuration and performance of the data assimilation system. Quart. J. Roy. Meteor. Soc., 137, 553-597.

Dunbar, R. S., T. Lungu, B. Weiss, B. Stiles, J. Huddleston, P. S. Callahan, G. Shirtliffe, K. L. Perry, C. Hsu, C. Mears, F. Wentz, and D. Smith, 2006: QuikSCAT science data product user's manual. Version 3.0, D-18053 - Rev A, Jet Propulsion Laboratory (JPL), USA, 85 pp.

Fiorino, M., 2002: Analysis and forecasts of tropical cyclones in the ECMWF 40-year reanalysis (ERA-40). 25th Conference on Hurricanes and Tropical Meteorology, CA, USA, 261–264.

Freidenreich, S. M., and V. Ramaswamy, 1999: A new multiple-band solar radiative parameterization for general circulation models. J. Geophys. Res., 104, 31389–31409.

Goody, R. M., 1952: A statistical model for water-vapour absorption. Quart. J. Roy. Meteor. Soc., 78, 165–169.

Harada, Y., H. Kamahori, C. Kobayashi, H. Endo, S. Kobayashi, Y. Ota, H. Onoda, K. Onogi, K. Miyaoka, and K. Takahashi, 2016: The JRA-55 Reanalysis: Representation of atmospheric circulation and climate variability, J. Meteor. Soc. Japan, 94, 269-302.

Ishii, M., A. Shouji, S. Sugimoto, and T. Matsumoto, 2005: Objective analyses of sea-surface temperature and marine meteorological variables for the 20th century using ICOADS and the KOBE collection. Int. J. Climatol., 25, 865–879.

Iwamura, K., and H. Kitagawa, 2008: An upgrade of the JMA operational global NWP model.

CAS/JSC WGNE Res. Activ. Atmos. Oceanic Modell., 38, 3–4.
JMA, 2002: Outline of the operational numerical weather prediction at the Japan Meteorological Agency. WMO Numerical Weather Prediction Progress Report. JMA, Japan, 158 pp.
JMA, 2007: Outline of the operational numerical weather prediction at the Japan Meteorological Agency. WMO Technical Progress Report on the Global Data-Processing and Forecasting System and Numerical Weather Prediction, JMA, Japan, 194 pp.
JMA, 2013: Outline of the operational numerical weather prediction at the Japan Meteorological Agency. Appendix to WMO Technical Progress Report on the Global Data-processing and Forecasting System (GDPFS) and Numerical Weather Prediction (NWP) Research, JMA, Japan, 188 pp.
Jones, P. D., D. H. Lister, T. J. Osborn, C. Harpham, M. Salmon, and C. P. Morice, 2012: Hemispheric and large-scale land surface air temperature variations: An extensive revision and an update to 2010. J. Geophys. Res., 117, D05127, doi:10.1029/2011JD017139.
Kalnay 2003: Atmospheric Modelling, Data Assimilation and Predictability. Cambridge University Press, UK, 341 pp.
Kalnay, E., M. Kanamitsu, R. Kistler, W. Collins, D. Deaven, L. Gandin, M. Iredell, S. Saha, G. White, J. Woollen, Y. Zhu, M. Chelliah, W. Ebisuzaki, W. Higgins, J. Janowiak, K. C. Mo, C. Ropelewski, J. Wang, A. Leetmaa, R. Reynolds, R. Jenne, and D. Joseph, 1996: The NCEP/NCAR 40-year reanalysis project. Bull. Amer. Meteor. Soc., 77, 437–471.
Kazumori, M., H. Owada, and K. Okamoto, 2004: Improvements of ATOVS radiance-bias correction scheme at JMA. CAS/JSC WGNE Res. Activ. Atmos. Oceanic Modell., 34, 15–16.
Kistler, R., E. Kalnay, W. Collins, S. Saha, G. White, J. Woollen, M. Chelliah, W. Ebisuzaki, M. Kanamitsu, V. Kousky, H. van den Dool, R. Jenne, and M. Fiorino, 2001: The NCEP-NCAR 50-year reanalysis: Monthly means CD-ROM and documentation. Bull. Amer. Meteor. Soc., 82, 247–267.
Kobayashi, C., H. Endo, Y. Ota, S. Kobayashi, H. Onoda, Y. Harada, K. Onogi, and H. Kamahori, 2014: Preliminary results of the JRA-55C, an atmospheric reanalysis assimilating conventional observations only. SOLA, 10, 78–82.
Kobayashi, S., Y. Ota, Y. Harada, A. Ebita, M. Moriya, H. Onoda, K. Onogi, H. Kamahori, C. Kobayashi, H. Endo, K. Miyaoka, and K. Takahashi, 2015: The JRA-55 reanalysis: General specifications and basic characteristics. J. Meteor. Soc. Japan, 93, 5–48.
Nakagawa, M., 2009: Outline of the high resolution global model at the Japan Meteorological Agency. RSMC Tokyo-Typhoon Center Technical Review, 11, JMA, Japan, 1–13.
NCDC, NWS, and FAA, 1981: NCDC TD3200 U.S. cooperative summary of day, 1890(1948)-cont. Research Data Archive at NCAR, Computational and Information Systems Laboratory, USA.
Okamoto, N., M. D. Yamanaka, S.-Y. Ogino, H. Hashiguchi, N. Nishi, T. Sribimawati, and A. Numaguchi, 2003: Seasonal variations of tropospheric wind over Indonesia: comparison between collected operational radiosonde data and NCEP reanalysis for 1992–99. J. Meteor. Soc. Japan, 81, 829–850.
Onogi, K., J. Tsutsui, H. Koide, M. Sakamoto, S. Kobayashi, H. Hatsushika, T. Matsumoto, N. Yamazaki, H. Kamahori, K. Takahashi, S. Kadokura, K. Wada, K. Kato, R. Oyama, T. Ose, N. Mannoji, and R. Taira, 2007: The JRA-25 reanalysis. J. Meteor. Soc. Japan, 85, 369-432.
Räisänen, P., 1998: Effective longwave cloud fraction and maximum-random overlap of clouds: a problem and a solution. Mon. Wea. Rev., 126, 3336–3340.
Rienecker M. M., M. J. Suarez, R. Gelaro, R. Todling, J. Bacmeister, E. Liu, M. G. Bosilovich, S. D. Schubert, L. Takacs, G.-K. Kim, S. Bloom, J. Chen, D. Collins, A. Conaty, A. da Silva, W. Gu, J. Joiner, R. D. Koster, R. Lucchesi, A. Molod, T. Owens, S. Pawson, P. Pegion, C. R. Redder, R. Reichle, F. R. Robertson, A. G. Ruddick, M. Sienkiewicz, and J. Woollen. 2011: MERRA: NASA's Modern-Era Retrospective Analysis for Research and Applications. J. Climate, 24, 3624-3648.

Roberts, R. E., J. E. A. Selby, and L. M. Biberman, 1976: Infrared continuum absorption by atmospheric water vapor in the 8-12-μm window. Appl. Opt., 15, 2085–2090.

Shibata, K., M. Deushi, T. T. Sekiyama, and H. Yoshimura, 2005: Development of an MRI chemical transport model for the study of stratospheric chemistry. Pap. Geophys. Meteor., 55, 75–119.

Thorne, P. W., D. E. Parker, S. F. B. Tett, P. D. Jones, M. McCarthy, H. Coleman, and P. Brohan 2005: Revisiting radiosonde upper air temperatures from 1958 to 2002. Journal of Geophysical Research, 110, D18105, doi:10.1029/2004JD005753.

Uppala, S. M., P. W. Kållberg, A. J. Simmons, U. Andrae, V. Da Costa Bechtold, M. Fiorino, J. K. Gibson, J. Haseler, A. Hernandez, G. A. Kelly, X. Li, K. Onogi, S. Saarinen, N. Sokka, R. P. Allan, E. Andersson, K. Arpe, M. A. Balmaseda, A. C. M. Beljaars, L. Van De Berg, J. Bidlot, N. Bormann, S. Caires, F. Chevallier, A. Dethof, M. Dragosavac, M. Fisher, M. Fuentes, S. Hagemann, E. Hólm, B. J. Hoskins, L. Isaksen, P. A. E. M. Janssen, R. Jenne, A. P. McNally, J.-F. Mahfouf, J.-J. Morcrette, N. A. Rayner, R. W. Saunders, P. Simon, A. Sterl, K. E. Trenberth, A. Untch, D. Vasiljevic, P. Viterbo, and J. Woollen, 2005: The ERA-40 re-analysis. Quart. J. Roy. Meteor. Soc., 131, 2961-3012.

van de Berg, L., J. Gustafsson, and A. Yildirim, 2002: Reprocessing of atmospheric motion vectors from Meteosat image data. ECMWF ERA-40 Project Report Series, 3, ECMWF, UK, 159–168.

WMO, 1986: A preliminary cloudless standard atmosphere for radiation computation, World Climate Programme (WCP), 112, 53 pp.

Zhong, W., and J. D. Haigh, 1995: Improved broadband emissivity parameterization for water vapor cooling rate calculations. J. Atmos. Sci., 52, 124–138.